C.P. No. 139
(15,348)
A.R.C. Technical Report

MINISTRY OF SUPPLY

AERONAUTICAL RESEARCH COUNCIL

CURRENT PAPERS

The Measurement of Heat Transfer and Skin Friction at Supersonic Speeds

Part III. Measurements of Overall Heat Transfer and of the Associated Boundary Layers on a Flat Plate at $M_1 = 2.43$

By

R. J. Monaghan and J. R. Cooke

LONDON: HER MAJESTY'S STATIONERY OFFICE

1953

Price 12s. 0d. net

CORRIGENDA

Section 6. Analysis of temperature profiles
Section 7. Effect of errors in temperature measurement

In both the above sections use is made of temperature-velocity distributions suggested by Squire[9]. These distributions incorporate the index "n" of the power law velocity distribution, which is normally of the order of 1/7. It must be stressed therefore that the curves labelled "n = 0" in Figures 20 - 24 have no physical significance and should only be regarded as giving an absolute lower (or upper) bound to the theoretical values.

Setting n = 0 in formulae such as for recovery factor is only justified on the grounds of its being a convenient and (in most cases) sufficiently accurate approximation.

28th September, 1953

C.P. 139

Technical Note No. Aero.2129

December, 1951

ROYAL AIRCRAFT ESTABLISHMENT

The measurement of heat transfer and skin friction at supersonic speeds

Part III - Measurements of overall heat transfer and of the associated boundary layers on a flat plate at $M_1 = 2.43$

by

R. J. Monaghan
and
J. R. Cooke

SUMMARY

Results are given of overall heat transfer measurements and of pitot and thermocouple traverses of the associated boundary layers on a flat plate at $M_1 = 2.43$.

A mean value of 0.906 was obtained for temperature recovery factor and the overall heat transfer measurements from plate to stream agreed well with the formula

$$k_{hw} = 0.045 \left(Re_w \frac{T_1}{T_w} \right)^{-1/5}$$

which is the modification of a known low speed formula in accordance with the results of Ref.2.

There was some forward movement of boundary layer transition, a variation in the exponent of the turbulent velocity distribution and an increase in displacement thickness with heat transfer. However, no decrease in skin friction below its zero heat transfer value was found.

Under zero heat transfer conditions the temperature distribution across the boundary layer varied as the square of the velocity distribution. For a given free stream temperature, the difference between zero heat transfer and heat transfer temperature distributions showed an approximately linear variation with velocity.

LIST OF CONTENTS

		Page
1	Introduction	4
2	Experimental apparatus	4
2.1	Improvement of heating system	4
2.2	Static pressure measurement	5
2.3	Measurement of plate temperature	5
2.4	Pressure and temperature measurement in the boundary layer	5
2.5	Pitot tube traversing gear	6
2.6	Mechanical indication of transition	6
3	Flow conditions over plate during tests	6
3.1	Mach number distributions	6
3.2	Surface temperature distributions	7
3.3	Movement of boundary layer transition with heat transfer	8
4	Measurements of kinetic temperature and of overall heat transfer	9
4.1	Kinetic temperature	9
4.2	Overall heat transfer	10
5	Boundary layer measurements	12
5.1	Velocity and temperature distributions	12
5.2	Displacement and momentum thicknesses	13
5.3	Mean skin friction	15
5.4	Log law velocity profiles	16
6	Analysis of temperature profiles	17
6.1	Zero heat transfer conditions	18
6.2	With heat transfer	19
6.3	Effect of errors in temperature measurement	21
7	Conclusions	23
List of Symbols		24
References		26

LIST OF APPENDICIES

	Appendix
Traversing pitot thermocouple	I
Mechanical indication of transition	II
Formulae used for comparison with experimental results	III

LIST OF TABLES

	Table
Measurement of kinetic temperature	I
Measurements of overall heat transfer	II
Measurements of turbulent boundary layer on flat plate with heat being transferred	III

LIST OF ILLUSTRATIONS

	Figure
General arrangement of tunnel	1
Location of pressure points, thermocouples and pitot traverse holes	2
Absolute micro-manometer	3
Traversing pitot thermocouple	4
Details of pitot tube traversing gear	5
Transition indication instrument ("Creeper")	6
General views of tunnel	7
Mach number distributions along plate	8
Surface temperature distributions on plate	9
Movement of boundary layer transition with heat transfer	10
Variation of overall heat transfer coefficient	11
Temperature and velocity distributions in boundary layer	12
Displacement and momentum thicknesses	
T_w = 373°K T_{H_1} = 276.5°K	13
T_w = 373°K T_{H_1} = 237°K	14
Zero heat transfer (Ref.2)	15
Ratio of displacement to momentum thickness	16
Mean skin friction coefficient C_F	17
Mean skin friction coefficient C_{F_w}	18
Log law velocity distributions	19
(Total temperature) - velocity distributions	20
Collapsed total temperature - velocity distributions	21
Collapsed static temperature - velocity distributions	22
Total temperature - velocity distribution, zero heat transfer (enlarged from Fig.20)	23
Energy distributions across boundary layer	24

1 Introduction

This note forms part of a series giving the results of an investigation of the boundary layer on a flat plate mounted in one wall of a 5" x 5" supersonic wind tunnel, with and without heat transfer. In the former case, direct measurements are also made of the overall heat transfer rates.

The first note[1] gave details of the tunnel and equipment and the results of preliminary tests, made at a Mach number of approximately 2.5, with the plate in the tunnel wall boundary layer.

The second[2] gave details of the removal of this boundary layer by suction at the leading edge of the plate and subsequent pitot measurements of the plate boundary layer under zero heat transfer conditions.

At this stage the nozzle was redesigned to give more uniform flow conditions in the working section, and the results of check tests of the zero heat transfer boundary layer were included in the second note[2]. The tests were then continued with heat being transferred and the present note gives the results of overall heat transfer tests and of pitot and thermocouple traverses of the boundary layers associated with them. The mean Mach number over the plate is now 2.43.

A subsequent note will give the results of check tests at $M = 2.82$.

2 Experimental Apparatus

The general arrangement of the tunnel as set up for the present tests at $M = 2.43$ was modified slightly from that described in Ref.1 and is as shown in Figs.1 and 2. General views of the tunnel and equipment are shown in Figs.7a and 7b.

A single sided nozzle is now used and the copper hot plate is mounted in the flat wall. The tunnel axis is horizontal and the hot plate is vertical. Details of the latter and of the heating system are as given in Ref.1 and the suction slot follows the design used in Ref.2.

2.1 Improvement of heating system

Tests had shown that the largest single source of tare loss in the heating system as described in Ref.1 was from the boiler. Furthermore, this loss varied with the condition and packing of the cork and kapok then used for insulation.

The heat loss from the boiler was therefore reduced by surrounding it with a coil of copper tubing through which steam at atmospheric pressure was passed. Fig.1 shows the system of lagging adopted. By this means the tare loss of the whole system was kept down to 0.004 ± 0.002 kcal/sec, which was always less than 1 per cent of the net heat transferred to the air stream from the hot plate. Care was taken to keep the pressure low in the coils in order not to transmit heat to the boiler and steam was circulated in them for about half an hour before the beginning of a test in order to heat the lagging.

2.2 Static pressure measurement

Static pressures were measured at points on the plate indicated in Fig.2 and the manometer system was the same as described in Ref.1 except that the sloping gauge was replaced by an absolute micro-manometer (Fig.3). This was used to measure the reference pressure in each bank of water manometers through a four-way connection.

The scale is graduated in millimetres with a vernier reading to 0.05 mm, and an optical system is used for sighting the level of the meniscus. To prevent contamination of the mercury, a glass wool filter and a silica gel drier are fitted in the pipe-line.

2.3 Measurement of plate temperature

The surface temperatures of the plate were measured at the points indicated on Fig.2 using manganin-constantan thermocouples set in the plate as described in Ref.1. The readings were taken with a Tinsley constant resistance potentiometer and mirror galvanometer, which has a least count of 0.01°C.

2.4 Pressure and temperature measurement in the boundary layer

To obtain pitot pressure and total temperature measurements in the boundary layer and to ensure that these would be made at the same points, a traversing pitot-thermocouple (Fig.4) was designed. Full details of its construction and performance are given in Appendix I.

The instrument consists of a small diameter pitot head made from quartz tubing, with a thermo-junction placed inside it. Pitot pressures are read in the ordinary way by connecting the tube to a manometer, but when measuring temperatures a vacuum pump is connected to the tube to induce a small flow of air over the thermo-junction to raise the heat transfer rate to the thermocouple and reduce the effect of heat losses to the shield. In this way recovery factors of over 89 per cent were obtained even for tubes as small as 0.005 in. diameter at the tip, the recovery factor (β) being defined by

$$\beta = \frac{T_{th} - T}{T_H - T}$$

where T is the static temperature of the stream tube

T_H is its total temperature

and T_{th} is the thermocouple reading.

Further details of the calibration of the tubes are given in Appendix I.

Pitot pressures were read to within 0.01 in. on a mercury gauge fitted with sighting wires and vernier scale (Fig.7b) and temperatures were measured on the Tinsley potentiometer (Fig.7a) which under test conditions of fluctuating temperature enabled readings to be made to within 0.05°C.

2.5 Pitot tube traversing gear

The pitot tube traversing gear was similar to that described by Lukasiewicz and Royle[3], but for convenience it is shown in Fig.5. A general view of the installation is shown in Fig.7b.

Considerable difficulty was experienced at stagnation temperatures below -30°C, both in the traversing gear and in the pitot response rate. The former froze solid, but this difficulty was overcome by steam jacketing the holder (Fig.5).

The poor response of the pitot was attributed to "snow" in the tunnel air creating an ice blockage at its mouth. Support for this explanation was given by a curious shot blasting effect noticed on the support tube after a number of these low temperature runs. The pitot was freed by touching it on the hot plate and also by injecting ethyl alcohol, but these were only temporary cures.

2.6 Mechanical indication of transition

Only a limited amount of success was obtained[2] using chemical methods to indicate transition, so for the present tests a mechanism was designed to traverse a pitot tube along the plate as well as normal to it. Because of its method of operation, this instrument was called a "creeper" and full details of its construction are given in Appendix II and illustrated in Fig.6.

The instrument proved very successful and with it a quick survey of boundary layer state was possible. The fore-and-aft traverses were made with the tip of the pitot just touching the plate and in this way the curves of Fig.10 were obtained.

A disadvantage (as compared with the chemical method) was that the fore-and-aft traverse was confined to a single line. However, this was the line on which the normal pitot traverses were taken, so that the two types of traverse are directly comparable.

3 Flow conditions over plate during tests

Figs.8 and 9 show the Mach number and surface temperature distributions along the plate during the various tests. The Mach numbers were obtained by combination of the measured static pressures on the plate with the tunnel stagnation pressure. The temperatures are from direct measurement by the surface thermocouples.

Fig.10 shows the movement of boundary layer transition with heat transfer, as determined by the "creeper" traverses along the surface.

All the measurements are along the centre-line of the plate.

3.1 Mach number distributions

The full line in Fig.8b shows the longitudinal Mach number distribution at the position of the plate, but recorded on an unbroken flat wall. Comparison with the broken lines (recorded with the plate in position) shows that the plate introduces a disturbance which is evident on the centre line in the region of $x/\ell = 0.3$ (i.e. about four inches from the leading edge). Likely sources of this disturbance are the points where the leading edge of the plate enters the boundary layers on the side walls. This explanation is supported both by experiments[8]

made with a reflection plate spanning the working section of a supersonic wind tunnel and also by a transition photograph already published (Fig.13 of Ref.2) of the plate in the present tunnel. The latter shows the beginning of a disturbance at each corner and also that the transition region is tongue-shaped. Thus it is almost certain that the disturbance shown in Figs.8a and 8b is inherent in the general design and cannot be eliminated without extensive alterations.

Downstream of $x/\ell = 0.4$, Figs.8a and 8b show that the variation in Mach number was always within one per cent of a mean and this was considered satisfactory. There was no significant variation with stagnation temperature (T_{H_1}).

During the heat transfer tests (Fig.8a) the mean Mach number over the plate length (excluding the disturbance at $x/\ell = 0.3$) was 2.43 and for convenience this mean was taken to apply throughout the whole test series. (The different mean value exhibited by one of the zero heat transfer curves arises from a slight error in the spacing of the liners.)

3.2 Surface temperature distributions

3.21 Under zero heat transfer conditions

Under these conditions the temperature recovery factor (β) is defined by

$$\beta = \frac{T_w - T_1}{T_{H_1} - T_1} \qquad (1)$$

where T_w is the surface temperature of the plate

T_1 and T_{H_1} are static and total temperatures in the stream outside the boundary layer.

The theoretical value of β for a laminar boundary layer is 0.85 and the measured value for turbulent layers is approximately 0.90. Hence it might be expected that the surface temperatures at the front of the plate would be less than those at the back by about 8°C, when $M_1 = 2.43$.

Fig.9a shows the distribution measured when the interior of the plate was open to room air and the tunnel stagnation temperature was held at the level for zero overall heat transfer in accordance with the results of Section 4.1 below (which gives mean $\beta \simeq 0.90$). Contrary to expectation all the temperatures lie within 1°C of a mean value and, apart from the possibility of a slight rise at the very front ($x/\ell < 0.2$), they decrease uniformly from the leading edge to the trailing edge of the plate. However it should be noted that the measured[2] rate of growth of the "laminar" boundary layer over the forward portion of the plate was greater than theory would predict, so that the forward temperatures are not those of a true laminar layer.

3.22 During overall heat transfer measurements

Fig.9b shows that with steam in the plate the surface temperature distribution followed a definite pattern at all tunnel temperature levels. Furthermore the variation at each level is sufficiently small to justify the use of mean plate temperatures in the analysis of the test results.

Similar temperature distributions were obtained during the pitot traverse tests, when the plate was heated by process steam.

3.3 Movement of boundary layer transition with heat transfer

Fig.10 gives the results of the "creeper" traverses along the centre line of the plate and shows a definite forward movement of transition with increasing heat transfer from plate to stream. Based on distance from the leading edge of the plate to the beginning of the transition region, the Reynolds number of transition decreases from 0.55×10^6 through 0.35×10^6 to 0.34×10^6 as the temperature ratio T_w/T_{H_1} increases from 0.946 (zero heat transfer) through 1.37 to 1.60. This is in qualitative agreement with Lees theoretical result[4] that the addition of heat has a destabilising effect on the compressible laminar boundary layer.

For given Mach number and temperature conditions, Lees theory[4] gives a minimum critical Reynolds number ($R_{\theta_{cr}}$ based on momentum thickness) below which small disturbances will be damped out. Furthermore, for Reynolds numbers equal to the critical, the initial rate of amplification of such disturbances should vary approximately as the reciprocal of the root of $R_{\theta_{cr}}$. Combination of the two might therefore give an indication of the Reynolds number for transition (R_{θ_T}).

Values of $R_{\theta_{cr}}$ have been calculated using Ref.4 for the cases of Fig.10 and are compared in the following table with semi-empirical estimates of the order of R_{θ_T}. (The latter are based on the curves of Fig.10 and on theoretical estimates for the variation of θ in the compressible laminar boundary layer on a flat plate. The transition "points" were taken at the beginning of the transition regions indicated on Fig.10.)

T_w/T_{H_1} =	0.946	1.37	1.60
$R_{\theta_{cr}}$ = Theoretical	85.5	2.04	1.15
$1/\sqrt{R_{\theta_{cr}}}$ =	0.108	0.70	0.93
R_{θ_T} = Experimental	460	410	440

There is no correlation between these figures. In particular, the experimental movement of transition with heat transfer is too small, probably because transition in the zero heat transfer case occurs too early.

Lees also shows[4] that theoretically $R_{\theta_{cr}}$ can become infinite when the free stream is supersonic provided sufficient heat is withdrawn from the boundary layer. Some tests were therefore made with a tunnel stagnation temperature of approximately 313°K and a plate temperature of approximately 250°K, which conditions satisfied the

theoretical requirements for infinite $R_{\theta_{cr}}$ when $M_1 = 2.43$. (The low plate temperature was obtained by circulating alcohol cooled by Cardice (solid Carbon dioxide).) These tests were made before the "creeper" was available, but pitot traverses showed that at most the transition point had only moved back one inch.

However it is probable that in addition to free stream turbulence, both the corner disturbances referred to in Section 3.1 above and the residual turbulence left over from the tunnel wall boundary layer play major roles in determining transition, even on the centre-line, so that it is doubtful whether any appreciable lengthening of the laminar boundary layer could be achieved with the present rig. Attempts now being made to reduce the general turbulence level in the tunnel should help to clarify this point.

4 Measurements of kinetic temperature and of overall heat transfer

4.1 Kinetic temperature

This was measured using the experimental technique described in Ref.1. Briefly it consisted in measuring the inlet and outlet temperatures of room air circulating through the plate and in changing the tunnel stagnation temperature slowly until the outlet temperature equalled the inlet temperature, when zero heat transfer conditions were reached. Probably on account of the large heat capacity of the copper plate there is an appreciable time lag inherent in the system. As a result, zero heat transfer was reached at higher stagnation temperatures when the stagnation temperature was rising than when it was falling.

Table I gives the results of the measurements. When stagnation temperature (T_{H_1}) was rising, the mean value of T_{wo}/T_{H_1} was 0.943, where T_{wo} is the wall (plate) temperature for zero heat transfer. For falling T_{H_1}, the mean value of T_{wo}/T_{H_1} was 0.955. The overall mean value, which was subsequently used in the analysis of the heat transfer test results, was

$$\frac{T_{wo}}{T_{H_1}} = 0.949 .$$

The corresponding mean value for the temperature recovery factor, based on $M_1 = 2.43$ is

$$\beta = \frac{T_w - T_1}{T_{H_1} - T_1} = 0.906$$

This compares with the value

$$\beta = \sigma^{1/3}$$

$$= 0.896 \quad \text{when} \quad \sigma = 0.72$$

suggested by Squire[9] for turbulent boundary layers, where σ is the Prandtl number $(c_p\mu/k)$.

(The value for β obtained in the preliminary experiments[1] was 0.881.)

4.2 Overall heat transfer

Table II gives the results of the overall heat transfer measurements obtained by the same method as described in Ref.1. The plate was maintained at approximately 373°K and readings were taken over a range of tunnel stagnation temperatures from 233°K to 323°K.

The values for heat flow (Q) given in column 3 of the table are for the nett heat transferred from the plate to the air stream. As previously mentioned, the heat losses in the system did not exceed 0.004 ± 0.002 kcal/sec, which was always less than 1 per cent of the nett.

As in Ref.1 the mean heat transfer coefficient k_h is obtained from the formula

$$k_h = \frac{Q/S}{\rho_1 u_1 g c_p (T_w - T_{wo})}$$

where S is heated area of plate

ρ_1, u_1 are free stream density, velocity

g is acceleration due to gravity

c_p is specific heat of air at constant pressure (assumed constant)

T_w is wall (plate) temperature

and T_{wo} is wall (plate) temperature for zero heat transfer, obtained from stagnation temperature by the formula of Section 4.1.

(Note the change in notation from Ref.1 where T_w and T_{wo} were denoted by T_p and T_w respectively.)

The experimental values of k_h and the corresponding free stream Reynolds numbers (Re) based on plate length are given in Table II.

Now the results[2] of Part II of the present investigation suggested a formula for the variation of skin friction with Mach number and heat transfer. This is

when

$$\left.\begin{aligned} C_{F_i} &= C_{F_w} \\ Re_i &= Re_w \frac{T_1}{T_w} \end{aligned}\right\} \qquad (2)$$

where subscript "i" denotes incompressible values

subscript "w" denotes that density and viscosity are evaluated at wall temperature (T_w)

and T_1 is free stream static temperature.

The comparisons made in Ref.5 have shown that in subsonic flow through pipes with high heat transfer rates, the same formula might also be applied to the heat transfer coefficient k_h.

Application to the present case is handicapped by a scarcity of low speed results for heat transfer from a flat plate, and there is considerable scatter in those that are available[12]. The correlation given by a curve ascribed to Colburn in Ref.12, for $Re > 2 \times 10^4$ is

$$k_h \sigma^{2/3} = 0.036\ Re^{-1/5} \tag{3}$$

Modifying this equation in accordance with equation (2) and taking $\sigma = 0.72$, gives

$$k_{h_w} = 0.045 \left(Re_w \frac{T_1}{T_w}\right)^{-1/5} \tag{4}$$

as the corresponding compressible flow equation, or in terms of free stream density and viscosity,

$$k_h = 0.045\ Re^{-1/5} \left(\frac{T_1}{T_w}\right)^{\frac{2.16}{5}} \tag{4a}$$

wherein it is assumed that

$$\frac{\mu_1}{\mu_w} = \left(\frac{T_1}{T_w}\right)^{0.84} \tag{5}$$

as is approximately the case for the temperature range of the tests.

Equation (4a) suggests that the experimental values of $k_h\ Re^{1/5}$ should be plotted against T_1/T_w, or against T_{H_1}/T_w since T_1/T_{H_1} was constant during the tests. The latter has been done in Fig.11 which shows a definite variation in $k_h\ Re^{1/5}$ with temperature ratio T_{H_1}/T_w, and also that its mean value is considerably less than the low speed value 0.045. If, following equation (4a), we assume that

$$k_h\ Re^{1/5} \propto \left(\frac{T_{H_1}}{T_w}\right)^{\frac{2.16}{5}}$$

then application of the least squares method gives the curve of best fit to be

$$k_h\ Re^{1/5} = 0.032 \left(\frac{T_{H_1}}{T_w}\right)^{\frac{2.16}{5}} \tag{6}$$

as shown in Fig.11. Since for $M_1 = 2.43$ we have

$$\frac{T_1}{T_{H_1}} = 0.4585$$

then equation (6) is equivalent to

$$k_h\ Re^{1/5} = 0.0448 \left(\frac{T_1}{T_w}\right)^{\frac{2.16}{5}} \tag{6a}$$

and the constant is practically the same as that of equation (4a).

Thus equation (2) can be said to give a good correlation of the experimental results on the basis of a known incompressible flow formula. Obviously the agreement is dependent on the value of the constant in the latter, so that tests at other Mach numbers are required before a definite conclusion can be reached. This is emphasised by the fact that the experimental points in Fig.11 would be fitted better by a curve

$$k_h \, Re^{1/5} \propto \left(\frac{T_{H_1}}{T_w}\right)^{\frac{1.45}{5}}$$

than by the variation chosen above.

5 Boundary layer measurements

The results are given in Table III of pitot and thermocouple traverses of the turbulent boundary layer corresponding to two heat transfer rates given by $T_w = 373^oK$ and $T_{H_1} = 276.5^oK$ and 237^oK. Under these conditions the laminar boundary layer at the front of the plate was very short in extent (see Fig.10) and was found to be too thin for accurate measurement.

The measurements were analysed as in Ref.2 except that the density variations across the layer were obtained from the measured temperature distributions. A more detailed analysis of the temperature distributions themselves and of the effects of errors in them is given in Section 6 below.

A few pitot and thermocouple traverses were made of the zero heat transfer boundary layer to obtain the appropriate temperature distribution.

5.1 Velocity and temperature distributions

Representative turbulent velocity and temperature distributions for the two heat transfer conditions are given in Fig.12a and 12b. The faired power law curves giving the best fit with the experimental values were obtained by large scale log-plots of the experimental values.

Under zero heat transfer conditions the experimental velocity profiles were found[2] to follow the law

$$\frac{u}{u_1} = \left(\frac{y}{\delta}\right)^{1/7} \tag{7}$$

Under heat transfer conditions Figs.12a and 12b show that this is no longer the case. When $T_w/T_{H_1} = 1.35$ then (Fig.12a)

$$\left(\frac{u}{u_1}\right) = \left(\frac{y}{\delta}\right)^{1/6} \tag{8}$$

and when $T_w/T_{H_1} = 1.57$ then (Fig.12b)

$$\left(\frac{u}{u_1}\right) = \left(\frac{y}{\delta}\right)^{1/5} \tag{9}$$

Also shown in Figs.12a and 12b are the measured temperature distributions used in the analysis. Low speed measurements made by Elias[6] gave approximate identity between the distributions of u/u_1 and $(T_w - T)/(T_w - T_1)$, as is assumed in Reynolds analogy. The corresponding temperature function in compressible flow is

$$\Theta = \frac{T_w - T_H}{T_w - T_{H_1}} \tag{10}$$

and Figs.12a and 12b show that Reynolds analogy is not applicable. Further analysis is made in Section 6.

Fig.12c shows the results of the zero heat transfer measurements with pitot and thermocouple. Here the temperature distribution is of different form and this also will be considered in Section 6 below. The velocity distribution follows the 1/7th power law in shape as in Ref.2. The faired curve is the mean curve found in Ref.2, but in the present case a different value of δ^x/δ would give a better fit with the experimental values.

5.2 Displacement and momentum thicknesses

Values of displacement (δ^x) and momentum (θ) thicknesses are given in Table III and are plotted in Figs.13 and 14. For comparison, the zero heat transfer results of Ref.2 are reproduced in Fig.15.

The ratios (H) of displacement to momentum thickness are plotted in Fig.16 for all cases.

Now

when

$$\left.\begin{aligned} C_{F_i} &= C_{F_w} \\ Re_i &= Re_w \frac{T_1}{T_w} \end{aligned}\right\} \tag{2}$$

gives the compressibility variation suggested in Ref.2 for skin friction coefficient. Details are given in Appendix III of the application of this formula, in conjunction with the momentum equation and the suggested formula

$$\frac{H}{H_i} = \frac{T_w}{T_1} + \frac{\gamma-1}{2} \sigma^{\frac{1}{3}} M_1^2 \tag{11}$$

for the variation in H, to predict values of δ^x and θ appropriate to the temperature conditions of Figs.13 and 14. The resulting curves are shown in Figs.13 and 14 by the full lines labelled "Prediction of Ref.2".

(In obtaining these, the formula

$$C_{F_i} = 0.46 \, (\log Re_i)^{-2.6} \tag{12}$$

giving (by equation (2))

$$C_{F_w} = 0.46 \left(\log Re_w \frac{T_1}{T_w}\right)^{-2.6} \qquad (12a)$$

was chosen for skin friction coefficient since it is valid over a wider range of Reynolds number than the Blasius power law formula. However the position of the effective start of the turbulent boundary layer was determined as in Ref.1 using power law considerations.)

For constant Mach number, equation (11) predicts that H should increase if T_w/T_i is increased. The experimental results of Fig.16 show such an increase, although it is less than would be predicted by equation (11).

On the other hand, there is no agreement between the experimental and predicted values of δ^x and θ in Figs.13 and 14, both sets of predicted values being too low.

Now equations (11) and (13) gave good agreement with the experimental values of δ^x and θ in the zero heat transfer case (Fig.15). In power law form the curves of Fig.15 are approximated by

$$\theta = 0.0265\ Re_x^{-1/5}\ x \qquad (13)$$

and

$$\frac{\delta^x}{\theta} = H = 4.05$$

from equation (11). Figs.13 and 14 show that equation (13) also gives values of θ in good agreement with experiment under heat transfer conditions. Furthermore, reasonable estimates of δ^x are obtained by combination of equation (13) with the appropriate values of H from equation (11).

The conclusions to be drawn from the present experimental results are therefore that, at $M_1 = 2.43$,

(1) under zero heat transfer conditions, combination of the formula

$$C_{F_w} = 0.46 \left(\log Re_w \frac{T_1}{T_w}\right)^{-2.6} \qquad (12a)$$

with the momentum equation gives a good estimate of the variation of θ/x with Re_x,

(2) when heat is being transferred the same variation is valid, (this is contrary to the prediction of a decrease given by equation (12a))

and

(3) both with and without heat transfer, equation (11)

$$\frac{H}{H_i} = \frac{T_w}{T_1} + \frac{\gamma-1}{2} \sigma^{\frac{1}{3}} M_1^2 \qquad (11)$$

gives a reasonable estimate of the increase of H with increase of T_w/T_1 .

Against conclusion (2) it should be noted that the overall heat transfer results (Section 4 above) showed a variation of $k_h\, Re^{1/5}$ with T_w/T_1 , which might suggest that there should be a similar variation in skin friction (and hence in momentum thickness). Also, some skin friction measurements (Ref.7, analysed further in Ref.5) for subsonic flow through pipes have shown a definite decrease with increasing heat transfer from the wall. The present lack of decrease may be genuine, but since the flow over the plate is subject to disturbances (Section 3 above), there is always the possibility that these disturbances are masking any temperature effect.

5.3 Mean skin friction

Plots of mean skin friction coefficient against Reynolds number are given in Figs.17 and 18. The former is a plot of C_F and Re based on free stream density and viscosity, the latter of C_{F_w} and $Re_w\, T_1/T_w$ in accordance with the suggested formula (equation (2)) of Ref.2.

In the absence of pressure gradients

$$C_F = \frac{2\theta}{x} \quad . \tag{14}$$

and the experimental values were obtained in this manner. Thus Figs.17 and 18 only represent an alternative presentation of the momentum thickness plots of Figs.13-15.

Once again, equation (13)

$$C_{F_w} = 0.46 \left(\log Re_w \frac{T_1}{T_w} \right)^{-2.6} \tag{13}$$

was chosen for comparison, since in incompressible flow it is valid over a wider range of Reynolds number than the 1/5th power law formula.

Fig.17 shows the variation in C_F which would be given by equation (13) for the temperature conditions of the tests. No such variation was found experimentally but the predicted curves show that,

(1) at zero heat transfer the slope of the curve gives approximately

$$C_F \propto Re^{-1/5}$$

but

(2) when $T_w = 373^\circ K$ and $T_{H_1} = 237^\circ K$ the slope is approximately

$$C_F \propto Re^{-1/4.5} \quad .$$

This change in exponent would correspond in incompressible flow to a change in velocity profile from

$$\frac{u}{u_1} = \left(\frac{y}{\delta}\right)^{1/7}$$

to

$$\frac{u}{u_1} = \left(\frac{y}{\delta}\right)^{1/6}$$

and Fig.12b showed that the velocity profile changed to

$$\frac{u}{u_1} = \left(\frac{y}{\delta}\right)^{1/5}$$

This point is illustrated further by Fig.18 which shows the ranges of $Re_W \, T_1/T_W$ covered by the experiments and the points at which the slopes correspond to different power laws.

It is evident therefore that the changes in velocity profile shown by Figs.12a and 12b correspond, if only qualitatively, with the variation in skin friction given by

$$C_{F_W} = 0.46 \left(\log Re_W \frac{T_1}{T_W}\right)^{-2.6} \qquad (13)$$

5.4 Log-law velocity profiles

One of the major assumptions (see Appendix III) in the theory of Ref.2 was that the incompressible constants could be retained in the general log-law form for the velocity distribution near a wall

$$\frac{u}{u_\tau} = A + B \log \frac{y u_\tau}{\nu} \qquad (14)$$

provided density and viscosity were evaluated at wall temperature.

If so, then

$$u_\tau = u_{\tau_W} = \sqrt{\left\{\frac{\tau_o}{\rho_W}\right\}}$$

and local skin friction (τ_o) can be evaluated from the momentum equation

$$\frac{\tau_o}{\rho_1 \, u_1^2} = \frac{d\theta}{dx} \, .$$

Values of $d\theta/dx$ were estimated from the experimental curves for θ in Figs.13-15 and the resulting velocity profiles are shown in Fig.19.

The usual incompressible values for A and B are

$$A = 5.8 \quad \text{or} \quad 5.5$$

and

$$B = 5.5 \quad \text{or} \quad 5.75$$

but Fig.19 shows that contrary to the assumption of Ref.2, A decreases and B increases with increasing heat transfer from wall to air stream. (The zero heat transfer curve in Fig.19 is based on more extensive experimental evidence than the corresponding curve in Ref.2. This accounts for the reductions in value of A and B to 5.45 and 5.4 respectively.)

The actual values are

$M_1 = 2.43$ T_w/T_{H_1}	A	B
0.948	5.45	5.4
1.35	3.65	5.6
1.57	1.65	6.1

If the values of $d\theta/dx$ used in obtaining these profiles were 20 per cent too high in the case $T_w/T_{H_1} = 1.57$, then changing to the correct values would only alter A and B to 2.1 and 6.7 respectively. Thus errors in measurement alone could not account for the variation shown in the table and the assumption of Ref.2 is obviously inadequate. Further work, both experimental and theoretical, is needed to assess the extent and effects of its inadequacy.

6 Analysis of temperature profiles

The measured temperature profiles have already been considered in Section 5.1 above, in conjunction with Fig.12 which showed that Reynolds analogy did not apply. This is illustrated further by Fig.20, where total temperature is plotted against velocity and the experimental values for each temperature level all lie below the corresponding linear variation postulated by Reynolds analogy.

Nor is any correlation of the experimental results obtained when they are plotted in the form

$$\frac{T_w - T_H}{T_w - T_{H_1}} \quad \text{against} \quad \frac{u}{u_1} .$$

Included in this figure are results from a single test when heat was being transferred from the air stream to the plate ($T_w/T_{H_1} = 0.816$). In this case the diameter of the pitot tube was 0.020 inches, but at the

other temperature levels measurements were made with tubes ranging in diameter from 0.024 inches down to 0.004 inches and no significant size effect could be found, except possibly in the zero heat transfer case (see enlarged plot in Fig.23) where a traverse was made with an oversize tube (0.040" O.D.).

In the analysis of these results it is convenient to consider first the zero heat transfer profiles and second the profiles when heat was being transferred.

6.1 Zero heat transfer conditions

For this case Squire[9] has suggested a total temperature distribution equivalent to

$$\Theta_o = \frac{T_{wo} - T_H}{T_{wo} - T_{H_1}} = \frac{\sigma^{\frac{3n+1}{n+3}} - 1}{\sigma^{\frac{n+1}{n+3}} - 1} \left(\frac{u}{u_1}\right)^2 \qquad (15)$$

with

$$T_{wo} - T_{H_1} = \frac{u_1^2}{2\,Jg\,C_p} \left(\sigma^{\frac{n+1}{n+3}} - 1\right)$$

where σ is Prandtl number (assumed constant)

and n is given by the velocity profile $\frac{u}{u_1} = \left(\frac{y}{\delta}\right)^n$

(setting $n = 0$ for convenience in equations (15) gives the well known factor $\sigma^{\frac{1}{3}}$ for kinetic temperature rise.)

Experimental values of Θ_o are therefore plotted against $(u/u_1)^2$ in Fig.21a, which shows however that a mean line through them would not pass through the origin (and would not agree with either of the straight lines given by equation (15) with $\sigma = 0.72$ and $n = 0$ and $1/7$). However the experimental values are obtained by the division of two small quantities, so that small errors are greatly magnified. A better plot is given by Fig.22a which considers the static temperature distribution.

The static temperature distribution corresponding to equation (15) above given by Squire[9] is equivalent to

$$\frac{T_{wo} - T}{T_{wo} - T_1} = \sigma^{\frac{2n}{n+3}} \left(\frac{u}{u_1}\right)^2 \qquad (16)$$

with

$$T_{wo} - T_1 = \sigma^{\frac{n+1}{n+3}} \frac{u_1^2}{2\,Jg\,C_p}$$

and Fig.22a shows that the experimental points lie close to either of the lines given by equation (16) with

$$\sigma = 0.72 \quad \text{and} \quad n = 0, \ 1/7 .$$

If anything, the experimental values are more nearly parallel to the line for $n = 1/7$ and it can easily be verified that their displacement from it is equivalent to the corresponding displacement of the total temperatures in Fig.21a.

From equations (16), this result means that

$$T_{H'} = T + \sigma^{\frac{3n+1}{n+3}} \frac{u^2}{2 J g c_p} \qquad (17)$$

is nearly constant across the layer[*], whereas it is usually assumed that the total temperature

$$T_H = T + \frac{u^2}{2 J g c_p}$$

can be taken as constant.

Also shown on Fig.22a are the theoretical distributions given by Crocco[10] for the compressible laminar boundary layer on a flat plate under zero heat transfer conditions. For $u/u_1 < 0.8$, Ref.11 has shown that these are given approximately by

$$\frac{T_{wo} - T}{T_{wo} - T_1} = \sigma^{\frac{1}{2}} \left(\frac{u}{u_1}\right)^2 \qquad (18)$$

with

$$T_{wo} = T_1 + \sigma^{\frac{1}{2}} \frac{u_1^2}{2 J g c_p}$$

and the similarity of equations (16) and (18) is evident.

6.2 With heat transfer

Under zero heat transfer conditions it has been shown that

$$\theta_o \propto \left(\frac{u}{u_1}\right)^2$$

is approximately the case for either laminar or turbulent boundary layers.

---

[*] $T_{H'}$ is exactly constant according to equation (16) if $n = 0$.

For laminar boundary layers with heat transfer, Ref.11 shows that the temperature function

$$\frac{(T_w - T) - (T_{wo} - T)_o}{T_w - T_{wo}}$$

has an approximately linear variation with u/u_1, where

$$(T_{wo} - T)_o$$

is the zero heat transfer temperature distribution (given by equation (18)) consistent with the free stream temperature under consideration.

For the turbulent boundary layer with heat transfer it therefore seems reasonable to attempt a similar correlation*, i.e. to plot experimental values of

$$\frac{(T_w - T) - (T_{wo} - T)_o}{T_w - T_{wo}} \quad \text{against} \quad \frac{u}{u_1} .$$

This is done in Fig.22b, which shows a good correlation of the experimental results. (In deriving the experimental temperature function it was necessary to assume that $(T_{wo}-T)_o/T_1$ would not vary with T_1.)

Fig.21b shows that the total temperatures are correlated on the same basis just as well as the static temperatures.

Also shown on Figs.21b and 22b are

(1) the laminar distributions given by Crocco[9]
and
(2) the straight line

$$\frac{(T_w - T) - (T_{wo} - T)_o}{T_w - T_{wo}} = \sigma^{-\frac{1}{3}} \left(\frac{u}{u_1}\right) \qquad (19)$$

with $\sigma = 0.72$.

The latter (equation (19)) looks as if it might form a reasonable extrapolation to the wall of the experimental curve.

Further experimental evidence is needed before a temperature distribution can be defined with confidence but the present indication is that combination of equations (19) and (16) should give a reasonable

---

* The same conclusion can be reached from consideration of the incompressible (isothermal) turbulent boundary layer with heat transfer.

estimate. This is

$$T_w - T = \sigma^{-1/3} (T_w - T_{wo}) \frac{u}{u_1} + \sigma^{1/3}_{\sigma^{5/11}} \left(\frac{u^2}{2 Jg C_P} \right) \qquad (20)$$

for $n = \overset{o}{1/7}$.

Note that equation (20) is equivalent to

$$\frac{T_w - T_H'}{T_w - T_{H_1}'} = \sigma^{-1/3} \frac{u}{u_1} \qquad (21)$$

where T_H' is given by equation (17), i.e.

$$T_H' = T + \sigma^{\frac{3n+1}{n+3}} \frac{u^2}{2 Jg C_P} \qquad (17)$$

with $n = 0$ or $1/7$.

6.3 Effect of errors in temperature measurement

6.31 Zero heat transfer conditions

Fig.23 shows, on enlarged vertical scale, the various zero heat transfer total temperature distributions discussed in Section 6.1 and previously depicted in Fig.20. Squire's distribution[9] (equation (16)) for $\sigma = 0.72$ and $n = 1/7$ gives

$$\frac{T_H}{T_{H_1}} = 1$$

when

$$\frac{u}{u_1} = 0.88 \text{ approx.}$$

so that for $u/u_1 > 0.88$ an arbitrary extrapolation was made as shown.

Displacement, momentum and energy* thicknesses were then calculated from a typical pitot traverse, using the following temperature distributions:-

---

* Energy thickness is given by

$$\delta_E = \int_0^{\delta} \frac{\rho u}{\rho_1 u_1} \left(\frac{T_H}{T_{H_1}} - 1 \right) dy$$

and for zero heat transfer δ_E should be zero.

(1) mean experimental

(2) Squire, $n = 0$

(3) Squire, $n = 1/7$, and

(4) $T_H/T_{H_1} = 1$ as was assumed in Ref.2, (which corresponds to constant energy across the layer).

The results are given in the following table

Temperature Distribution	Experimental	Squire		$\frac{T_H}{T_{H_1}} = 1$
		$n = 0$	$n = 1/7$	
δ^x	0.0672	0.0672	0.0677	0.0676
θ	0.0181	0.0177	0.0169	0.0169
δ_E	-0.00242	-0.00172	+0.00032	-

These results show that while the maximum change in δ^x is less than 1 per cent, θ changes by 7 per cent, and the variation in δ_E is over 100 per cent, involving a change in sign.

Fig.24 shows the actual distributions of energy across the boundary layer, corresponding to the above values of δ_E. For zero heat transfer, δ_E should be zero, so that the positive and negative areas enclosed by each curve should cancel. Fig.24 shows that only in the case of Squire's curve for $n = 1/7$ is there a positive area, which is strong evidence in favour of this temperature distribution compared with the $n = 0$ and experimental distributions. (The value of δ_E is positive, but it could be made equal to zero by slight modification of the extrapolated portion of the $n = 1/7$ temperature distribution in Fig.23.)

Two main conclusions follow. First, if the $n = 1/7$ distribution is accepted, then the table shows that the simpler practice of assuming constant total energy across the boundary layer gives almost identical results to it for δ^x and θ. Second, if the correct temperature distribution is in doubt (as it still is), then deductions concerning the boundary layer will be more reliable if based on δ^x than if based on θ.

6.32 Under heat transfer conditions

Calculations of δ^x, θ and k_h have been made for the case $T_w/T_{H_1} = 1.57$ and $Re_x = 2.7 \times 10^6$ (8.05 inches from L.E.) using an experimental pitot traverse in conjunction with

(1) the associated experimental temperature distribution of Fig.20, and

(2) Reynolds analogy, (also shown in Fig.20).

The values of k_h were obtained from the energy thickness δ_E using the formula

$$k_h = \frac{T_{H_1}}{T_w - T_{wo}} \frac{\delta_E}{x}$$

and comparison is made in the following table between values of $k_h \, Re_x^{1/5}$ thus derived and the value for the same value of T_w/T_{H_1} obtained in the overall heat transfer tests (Fig.11).

Temperature Distribution	Experimental	Reynolds Analogy
δ^x	0.0599	0.0604
θ	0.0106	0.0102
k_h	0.00092	0.00118
$k_h \, Re_x^{1/5}$	0.0178	0.0228
$k_h \, Re^{1/5}$ from Fig.11	0.026	

Once again, values of δ^x are seen to be more reliable than values of θ and it is evident that choice of temperature distribution has considerable effect on the values of k_h. It is also obvious that neither distribution is satisfactory and reference to Fig.14 shows that the decrease in θ obtained from use of Reynolds analogy would be insufficient to make any alteration to the conclusions drawn from that figure.

In general therefore it is obvious that further work is necessary before definite conclusions can be reached concerning temperature distributions in the turbulent boundary layer and the present results should not be regarded as being more than part of a progress report.

7 Conclusions

For the flat plate at $M_1 = 2.43$.

(1) A mean value of 0.906 was obtained for temperature recovery factor (Table I), as compared with Squire's suggested value $\sigma^{\frac{1}{3}} = 0.896$ ($\sigma = 0.72$).

(2) There was some forward movement of transition with heat transfer from plate to stream (Fig.10).

(3) Overall heat transfer measurements from plate to stream agreed well with the formula

$$k_{h_w} = 0.045 \left(Re_w \frac{T_1}{T_w} \right)^{-1/5}$$

which is Colburn's formula for low speed flow (as presented by McAdams[12]) modified in accordance with the results of Ref.2.

Pressure and temperature measurements in the associated turbulent boundary layers were obtained with a specially designed pitot-thermocouple (Fig.4) which had a high temperature recovery factor. The technique is still being developed and the following are interim conclusions.

(4) The exponent $(1/n)$ in the expression

$$\left(\frac{u}{u_1}\right) = \left(\frac{y}{\delta}\right)^{1/n}$$

for velocity distribution varied from $1/7$ to $1/5$ over the test range of heat transfer rates (Fig.12).

(5) Displacement thickness increased, but there was no decrease in momentum thickness (or skin friction) with heat transfer.

(6) Reynolds analogy did not apply between the temperature and velocity distributions in the boundary layer (Figs.12 and 20). Instead (a) under zero heat transfer conditions (between plate and stream) the temperature distribution varied as the square of the velocity distribution (Fig.22a), and (b) for a given free stream temperature, the difference between zero heat transfer and heat transfer temperature distributions showed an approximately linear variation with velocity.

List of Symbols

x distance along plate from leading edge

y distance normal to plate

ℓ length of plate

δ full thickness of boundary layer

u velocity at a point in the boundary layer

u_1 velocity in stream outside boundary layer

u_τ friction velocity $\left\{= \left(\frac{\tau_o}{\rho_w}\right)^{\frac{1}{2}}\right\}$

τ_o local skin friction

F total skin friction on length x

ρ density

C_F mean skin friction coefficient $= F/\frac{1}{2}\rho_1 u_1^2 x$

T static temperature

List of Symbols (Contd.)

T_H total temperature

subscripts

1 denotes free stream value

w denotes plate surface (wall) value

w_o wall value for zero heat-transfer

Q overall heat transfer rate

S heated area of plate

$$h = \frac{Q/S}{T_w - T_{wo}}$$

$$k_h = \frac{h}{\rho_1 u_1 g C_p}$$

where g is acceleration due to gravity

C_p is specific heat of air at constant pressure

ν kinematic viscosity

Re Reynolds number based on plate length $\left(= \frac{u_1 \ell}{\nu_1}\right)$

Re_x Reynolds number based on length x $\left(= \frac{u_1 x}{\nu_1}\right)$

$$Re_w = \frac{u_1 \ell}{\nu_w}$$

R_θ Reynolds number based on momentum thickness of boundary layer

σ Prandtl number (taken as 0.72 for air)

δ^x displacement thickness of boundary layer

$$= \int_0^\delta \left(1 - \frac{\rho u}{\rho_1 u_1}\right) dy$$

ϑ momentum thickness of boundary layer

$$= \int_0^\delta \frac{\rho u}{\rho_1 u_1} \left(1 - \frac{u}{u_1}\right) dy$$

List of Symbols (Contd.)

δ_E energy thickness of boundary layer

$$= \int_0^{\delta} \frac{\rho u}{\rho_1 u_1} \left(\frac{T_H}{T_{H_1}} - 1 \right) dy$$

β temperature recovery factor

$$= \frac{T_{wo} - T_1}{T_{H_1} - T_1} \quad \text{for flat plate}$$

$$= \frac{T_{th} - T}{T_H - T} \quad \text{for thermocouple}$$

where T_{th} = measured temperature of thermocouple

$\Theta = \dfrac{T_w - T_H}{T_w - T_{H_1}}$ is temperature function analogous to velocity ratio u/u_1 according to Reynolds analogy.

REFERENCES

No.	Author	Title, etc.
1	J.E. Johnson and R.J. Monaghan	The measurement of heat transfer and skin friction at supersonic speeds. Preliminary results of measurements on a flat plate at a Mach number of 2.5. C.P. No.59 April, 1949
2	R.J. Monaghan and J.E. Johnson	The measurement of heat transfer and skin friction at supersonic speeds. Part II. Boundary layer measurements on a flat plate at M = 2.5 and zero heat transfer. C.P. No.64 December, 1949
3	J. Lukasiewicz and J.K. Royle	Boundary layer and wake observation in supersonic flow. R.& M.2613 October, 1948

REFERENCES (Contd.)

No.	Author	Title, etc.
4	Lester Lees	The stability of the laminar boundary layer in a compressible fluid. NACA Report No. 876. Washington. July 1947.
5	R.J. Monaghan	Comparison between experimental measurements and a suggested formula for the variation of turbulent skin friction in compressible flow. ARC Current Paper No.45. February, 1950.
6	Élias	Measurement of temperature in the boundary layer of a flat plate. ZAMM 9 (1929), 434-453, 10 (1930) 1-14.
7	W.H. Lowdermilk and M.D. Grele	Heat transfer from high temperature surfaces to fluids. II - Correlation of heat transfer and friction data for air flowing in Inconel tube with rounded entrance. NACA RM No. E8L03, TIB/1954. Washington. March, 1949.
8	A.O. Ormerod	An investigation of the disturbances caused by a reflection plate in the working section of a supersonic tunnel. R. & M.2799 November, 1950.
9	H.B. Squire	Heat transfer calculation for aerofoils. R & M No.1986, November, 1942.
10	L. Crocco	Laminar boundary layer in gases (Lo strato limite laminare nei gas). ACA Monografir Scientifiche di Aeronautica, No.3, Rome, December, 1946. RAE Library Translation No.218. December, 1947.
11	R.J. Monaghan	An approximate solution of the compressible laminar boundary layer on a flat plate. R & M No.2760. November, 1949.
12	W.H. McAdams	Heat Transmission. Second Edition. p.206. McGraw-Hill. 1942.

APPENDIX I

Traversing Pitot Thermocouple

To measure the temperature distribution in the boundary layer traversing Pitot Thermocouples were made up and one is shown in Fig.4.

Requirements

The requirements for taking temperature measurements in a boundary layer on the Copper Hot Plate were:-

(1) an air flow over the thermocouple to give a high recovery factor,

(2) a Pitot Head of small diameter since the Boundary Layer is very thin, (only of the order of 0.2" even at the end of the plate),

(3) temperature and pressure readings to be taken by means of a single tube (both temperature and pressure readings are then guaranteed to be at the same point in the boundary layer).

The traversing Pitot Thermocouple described in this Appendix was made to fulfil the above requirements.

The traversing gear used was the same as for Pitot Tubes and the "Creeper". The E.M.F. of the thermocouple was measured on the same Tinsley Constant Resistance Potentiometer as used for the couples in the plate and the stagnation temperature thermocouple.

A Copper-Constantan couple was used, giving one microvolt for a temperature difference of the order of 0.025°C. Readings are therefore obtainable to within 0.01°C, but the accuracy under test conditions was nearer ± 0.05°C due to flow fluctuations.

Construction

Two main sizes of Pitot Thermocouple were made, the main difference being in the thickness of the thermo-junction wires and the Pitot Head Diameter. The first type had thermo-junction wires of 0.004" diameter and a pitot head of 0.020" outside diameter. The second type (as shown in Fig.4) had 0.002" diameter thermo-junction wires and a head of from 0.005" to 0.010" outside diameter.

The method of construction was much the same in both cases, the wires being threaded through the supporting inner glass and quartz tubes to insulate them from the steel supporting tubes. It should be pointed out that the wires are themselves insulated with a shellac type coat and are also silk covered but the inner glass and quartz tubes help in assembly and are an added insulating medium. The couple is threaded into the quartz pitot head; the head is then inserted into the 1.5 mm stainless steel tube and sealed into it. The thermocouple wires are retracted as the head is inserted in the 1.5 mm tube. This is to take up any slack and counter any possibility of the wires rubbing and causing a short circuit back in the support tube. Extreme care had to be taken to ensure that the couple remained near to the tip of the head and that the small couple wires did not snap - this being particularly difficult in the case of the 0.002" wires.

The seal is made by coating the quartz with platinum (liquid platinum process) copper plating this coat and then soft soldering the

joint. This method has been very successful and if reasonable care is taken an airtight joint should be obtained.

At the other end of the support tube the wires fit into a glass seal which also contains a lead to the manometer. The seal here is by a straight fusion of metal to glass.

In between the lead and the manometer a T-piece is inserted and a connection made to a vacuum pump. When this by-pass is open air flows over the thermocouple wires and through the by-pass - the thermocouple then having quite a good recovery factor. When this by-pass is closed the pressure in the traversing tube rises to give the total head. By this means it is possible to obtain readings of temperature and pressure at the same position (and nearly the same time).

Performance

Typical temperature recovery factors obtained with different sizes of pitot head are listed in the table below. Recovery factor is defined by

$$\beta = \frac{T_{th} - T}{T_H - T}$$

where T is the static temperature of the stream tube

T_H is its total temperature

and T_{th} is the thermocouple reading.

O.D. of tip of pitot head (inches)	0.075	0.040	0.020	0.0085	0.005
β	0.995	0.970	0.960	0.920	0.898

The majority of the measurements were made with tips of 0.020" diameter and less. These recovery factors were measured in the free stream and it had to be assumed that they would remain constant through the boundary layer.

A rough check was made of radiation effects by mounting a vertical steam heated copper plate and a pitot thermocouple in an evacuated flask. There was no rise in thermocouple temperature until it was only a few thousandths of an inch from the plate, and by directing a small air jet at the pitot head this rise could be delayed until the shield was touching the plate.

However the whole technique is still under development and systematic tests of the various effects have yet to be made.

Acknowledgment

The authors would like to acknowledge the help of Mr. McLennan of Chemistry Department, R.A.E., who demonstrated to them the use of the platinum-copper seal.

APPENDIX II

Mechanical Indication of Transition

Following the tests with a chemical coating to indicate the position of transition from laminar to turbulent flow as given in Appendix I of Ref.2 it was decided to try and obtain this by a Mechanical method.

Requirements

In order to traverse the transition region an instrument had to be designed that could fulfil the following requirements:-

(a) be inserted with the tunnel in position, i.e. go through a 0.75" diameter hole in a liner 2.25" thick,

(b) give a length of traverse slightly greater than the distance between the pitot traverse holes (Fig.2) so that the complete range of transition could be covered, and

(c) be sufficiently rigid to prevent vibration troubles.

Construction

An instrument, which because of its method of operation is called a "Creeper" was made and is shown in Fig.6. It had been found that 1 mm stainless steel hypodermic tubing (used for pitot heads) could be flexed to a small radius and still retain its elasticity. By enclosing a length of this tubing in a sheath, but, leaving it free to slide, it was possible to traverse the pitot longitudinally as well as vertically.

Two main points had to be watched in making the instrument, first that the pitot carrying tube should be a good sliding fit in the guide tube to eliminate vibration, and secondly that the guide peg should be a good fit in its slot, to prevent rotation. Copper was used for the radius portion of the instrument as the 1 mm hypodermic tube has to be inserted prior to setting. Copper in its annealed condition can be cold set and no heating is necessary (heating would have destroyed the elasticity of the hypodermic tube).

The pitot head is traversed by rotating the traverse operating tube so that pressure is exerted on the collar and transmitted through the 1 mm hypodermic tubing to the pitot carrying tube. The traverse operating tube carries an insert threaded $\frac{1}{4}$" B.S.F. 26 T.P.1. When hard against either of the collars, one revolution of the traverse operating tube will move the pitot head 0.0384". By setting the zero point by one of the thermocouple junctions or pressure points on the plate it was then possible to obtain the position of the pitot at any point on the traverse. Provided that each traverse was made continuously in one direction, the same accuracy was obtainable either way (a new zero was set before each traverse to allow for backlash in the thread and between the two collars).

Creeper traverses taken with this instrument are shown in Fig.10, the transition region being clearly marked.

The advantages of this instrument may be summed up as follows:-

(1) it does give a clear indication of transition (on a single line),

(2) it is easily made and providing sloppiness in vital parts is avoided gives an accuracy within the limits of the test,

(3) it can be inserted or removed from the tunnel easily and despite its length does not show any vibration tendency except at full traverse when a slight surging on the mercury U tubes is noted

and

(4) pitot traverses across the boundary layer can be taken at any point (on the single line) by using this instrument.

Disadvantages (as compared with chemical indication of transition) are,

(1) the indication of transition is limited to a single line as opposed to the overall picture given by a chemical method (Ref.2, Fig.13),

and

(2) any increase in length or cranking to give indication on an off centre line would bring about vibration and the need for a steady, thereby introducing complications to the present simple and easy method of mounting.

In general this instrument has proved successful and is a very useful additional piece of tunnel equipment.

APPENDIX III

Formulae used for comparison with the experimental results

The results[2] of Part II of the present investigation suggested the following formula for the variation of turbulent skin friction with Mach number and heat transfer,

$$\left.\begin{aligned} C_{F_i} &= C_{F_w} \\ \text{when} \quad Re_i &= Re_w \frac{T_1}{T_w} \end{aligned}\right\} \qquad \text{III.1}$$

where subscript "i" denotes incompressible values

subscript "w" denotes that in the compressible case density and viscosity are evaluated at wall temperature (T_w)

and T_1 is free stream static temperature.

This formula was based on the assumptions,

(1) that Reynolds analogy between momentum and heat exchange was valid

and

(2) that the incompressible constants could be retained in the general log-law form for the velocity distribution near a wall

$$\frac{u}{u_\tau} = A + B \log \frac{y u_\tau}{\nu} \qquad \text{III.2}$$

provided density and viscosity were evaluated at wall temperature.

The same analysis gave

$$\frac{H}{H_i} = \frac{T_w}{T_1} + \frac{\gamma-1}{2} M_1^2 \qquad \text{III.3}$$

(where H is the ratio δ^*/θ) but comparison with experimental data and the nature of assumption (1) above suggests that a better form would be

$$\frac{H}{H_i} = \frac{T_w}{T_1} + \frac{\gamma-1}{2} \sigma^{1/3} M_1^2 \qquad \text{III.4}$$

Application of formulae

1 Skin friction

If we take the incompressible formula

$$C_{F_i} = 0.46 \, (\log Re_i)^{-2.6}$$

for mean skin friction coefficient, then application of the formula III.1 gives

$$C_{F_w} = 0.46 \left(\log Re_w \frac{T_1}{T_w}\right)^{-2.6} \qquad \text{III.5}$$

as the corresponding formula for compressible flow.

Under the experimental conditions of the tests,

$$\left(\frac{\mu_1}{\mu_w}\right) \simeq \left(\frac{T_1}{T_w}\right)^{0.84} \qquad \text{III.6}$$

and hence in terms of free stream density and viscosity equation III.5 becomes

$$C_F = 0.46 \frac{T_1}{T_w} \left(\log Re + 2.84 \log \frac{T_1}{T_w}\right)^{-2.6} \qquad \text{III.6}$$

which is the form applied in Section 5.3 of the main report.

On the other hand, the Blasius formula

$$C_{F_1} = 0.074\, Re_i^{-1/5}$$

when combined with formula III.1 gives

$$C_{F_w} = 0.074 \left(Re_w \frac{T_1}{T_w}\right)^{-1/5} \qquad \text{III.7}$$

or in terms of free stream conditions

$$C_F = 0.074\, Re^{-1/5} \left(\frac{T_1}{T_w}\right)^{\frac{2.16}{5}} \qquad \text{III.8}$$

2 Momentum thickness

If there are no pressure gradients the momentum equation for flow over a flat plate gives

$$C_F = \frac{2\theta}{x} \qquad \text{III.9}$$

where θ is momentum thickness given by the integral

$$\theta = \int_0^{\delta} \frac{\rho u}{\rho_1 u_1} \left(1 - \frac{u}{u_1}\right) dy \qquad \text{III.10}$$

Combination of equations III.6 and III.9 then gives the variations in momentum thickness used in Section 5.2 of the main report.

3 Displacement thickness

Displacement thickness δ^x, given by

$$\delta^x = \int_0^\delta \left(1 - \frac{\rho u}{\rho_1 u_1}\right) dy \qquad \text{III.11}$$

can then be estimated from the values of the momentum thickness by use of equation III.4, i.e.

$$\frac{H}{H_i} = \frac{T_w}{T_1} + \frac{\gamma-1}{2} \sigma^{1/3} M_1^2 \qquad \text{III.4}$$

For the comparisons of Section 5.2 the values

$$H_i = 1.3$$

$$\sigma = 0.72$$

and $$M_1 = 2.43$$

were used.

TABLE I

Measurement of Kinetic Temperature

$M_1 = 2.43$

(Under zero heat transfer conditions, when $T_{IN} = T_{OUT}$, it is assumed that wall temperature $T_{wo} = T_{IN} = T_{OUT}$)

T_{wo} °K	T_{H_1} °K	$\frac{T_{wo}}{T_{H_1}}$	$\beta = \frac{T_w - T_1}{T_{H_1} - T_1}$	Direction of change of stagnation temperature T_{H_1}
292.8	311.0	0.941	0.891	Ascending
291.6	309.4	0.942	0.893	
288.8	305.5	0.945	0.898	
Mean ascending		0.943	0.894	
291.9	305.4	0.956	0.919	Descending
291.5	305.7	0.954	0.915	
Mean descending		0.955	0.917	
Overall mean		0.949	0.906	

TABLE II

Measurements of Overall Heat Transfer

(Table is arranged in chronological order. Divisions occur between each complete set of test runs)

$M_1 = 2.43$ $T_{wo}/T_{H_1} = 0.949$

Plate Length (ℓ) = 13.4 in = 0.340 metres
Heated Area (S) = 57.6 sq in = 3.72×10^{-2} sq metres

Plate Temp. ^oK	Stagn. Temp. T_{H_1} ^oK	Heat Flow $Q \times 10^2$ kcal/sec	* $h \times 10^2$ k cal / m^2 . sec . ^oC	$k_h \times 10^3 = h/\rho_1 u_1 g C_P$	Re $\times 10^{-6}$	$k_h \, Re^{1/5} \times 10^2$	T_{H_1}/T_w
372.8	292.6	11.34	3.20	1.45	3.33	2.92	0.7845
372.8	292.3	11.41	3.21	1.45	3.34	2.92	0.7835
371.1	273.0	12.85	3.08	1.34	3.70	2.77	0.732
371.6	273.0	13.04	3.11	1.36	3.70	2.79	0.732
373.2	323.0	7.76	3.13	1.44	2.96	2.84	0.866
373.1	322.8	7.97	3.20	1.48	2.96	2.91	0.865
373.1	233.0	17.25	3.05	1.21	4.71	2.63	0.6245
373.0	233.0	17.36	3.07	1.22	4.71	2.65	0.625
372.7	242.5	16.52	3.11	1.30	4.33	2.75	0.650
372.6	241.8	16.07	3.02	1.26	4.33	2.67	0.648
372.3	232.6	17.05	3.02	1.23	4.60	2.65	0.6235
372.3	232.5	17.16	3.04	1.24	4.60	2.67	0.6235
372.6	263.2	13.95	3.05	1.325	3.83	2.75	0.706
372.6	263.1	13.97	3.05	1.325	3.83	2.75	0.7055

TABLE II (Contd.)

Plate Temp. T_w ^oK	Stagn. Temp. T_{H_1} ^oK	Heat Flow $Q \times 10^2$ kcal/sec	* $h \times 10^2$ $\frac{k\ cal}{m^2 . sec . ^oC}$	$k_h \times 10^3 = h/\rho_1 u_1 g C_P$	Re $\times 10^{-6}$	$k_h Re^{1/5} \times 10^2$	T_{H_1}/T_w
372.6	283.0	11.94	3.08	1.38	3.46	2.81	0.759
372.7	283.0	11.87	3.06	1.37	3.46	2.79	0.758_5
373.0	293.8	11.06	3.16	1.44	3.31	2.90	0.787_5

* $$h = \frac{Q}{S\,(T_w - T_{wo})}$$

TABLE III

Measurements of turbulent boundary layer on flat plate with heat being transferred

$M_1 = 2.43$

x = distance downstream from leading edge of plate

(a) $T_w = 373^\circ K$ $T_{H_1} = 276.5^\circ K$ $T_1 = 127^\circ K$

x Inches	$Re_x \times 10^{-6}$	δ^x Inches	θ Inches	$H = \frac{\delta^x}{\theta}$	$C_F = \frac{2\theta}{x}$	Tube Dia. inches
4.20	1.19	0.0306	0.0067	4.57	0.0032	0.020
5.90	1.60	0.0403	0.0084	4.80	0.0028_5	0.020
8.00	2.05	0.0502	0.0100	5.02	0.0025	0.020
8.30	2.30	0.0534	0.0118	4.53	0.0028_5	0.009
10.75	2.70	0.0712	0.0140	5.09	0.0026	0.020
11.05	2.77	0.0730	0.0140	5.21	0.0025_5	0.009
12.85	3.40	0.0830	0.0171	4.85	0.0026_5	0.020

(b) $T_w = 373^\circ K$ $T_{H_1} = 237^\circ K$ $T_1 = 109^\circ K$

x Inches	$Re_x \times 10^{-6}$	δ^x Inches	θ Inches	$H = \frac{\delta^x}{\theta}$	$C_F = \frac{2\theta}{x}$	Tube Dia. inches
2.45	0.84	0.0196	0.0035	5.60	0.0028_5	0.020
4.25	1.42	0.0382	0.0067	5.70	0.0031_5	0.020
6.00	2.12	0.0446	0.0085	5.25	0.0028	0.020
8.05	2.71	0.0599	0.0106	5.65	0.0026_5	0.020
10.80	3.70	0.0743	0.0133	5.58	0.0024_5	0.020
12.90	4.39	0.0855	0.0164	5.21	0.0025_5	0.020

Wt.2078. CP139. K3. - Printed in Great Britain.

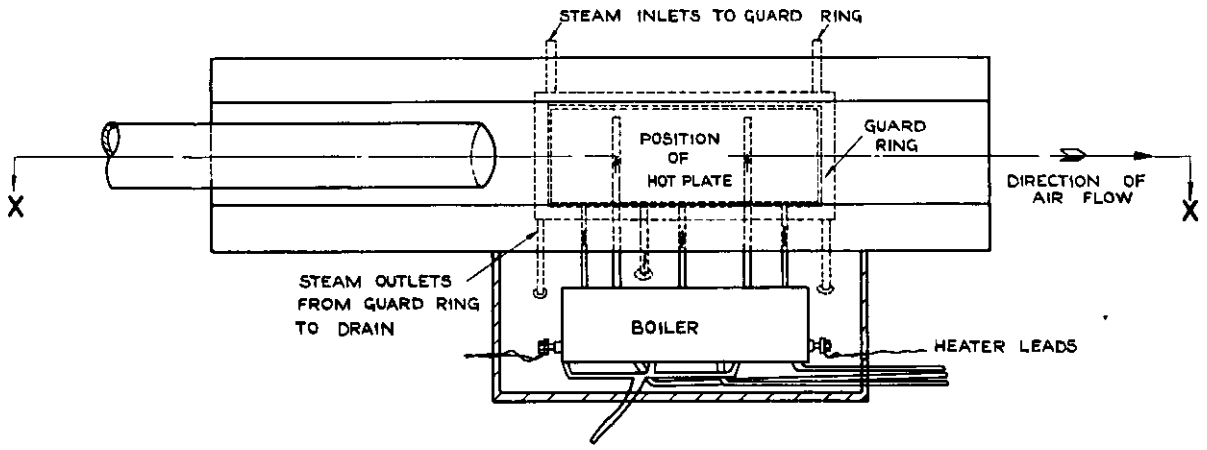

SIDE ELEVATION.

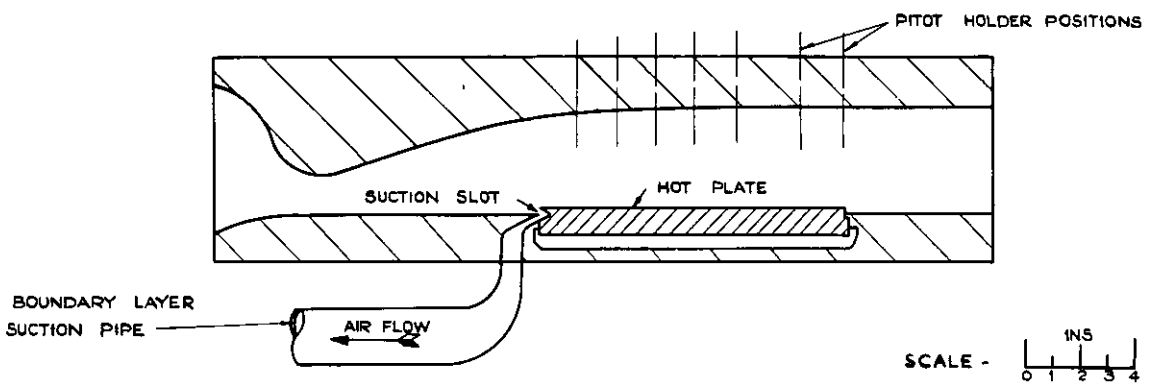

SECTION ON X-X.

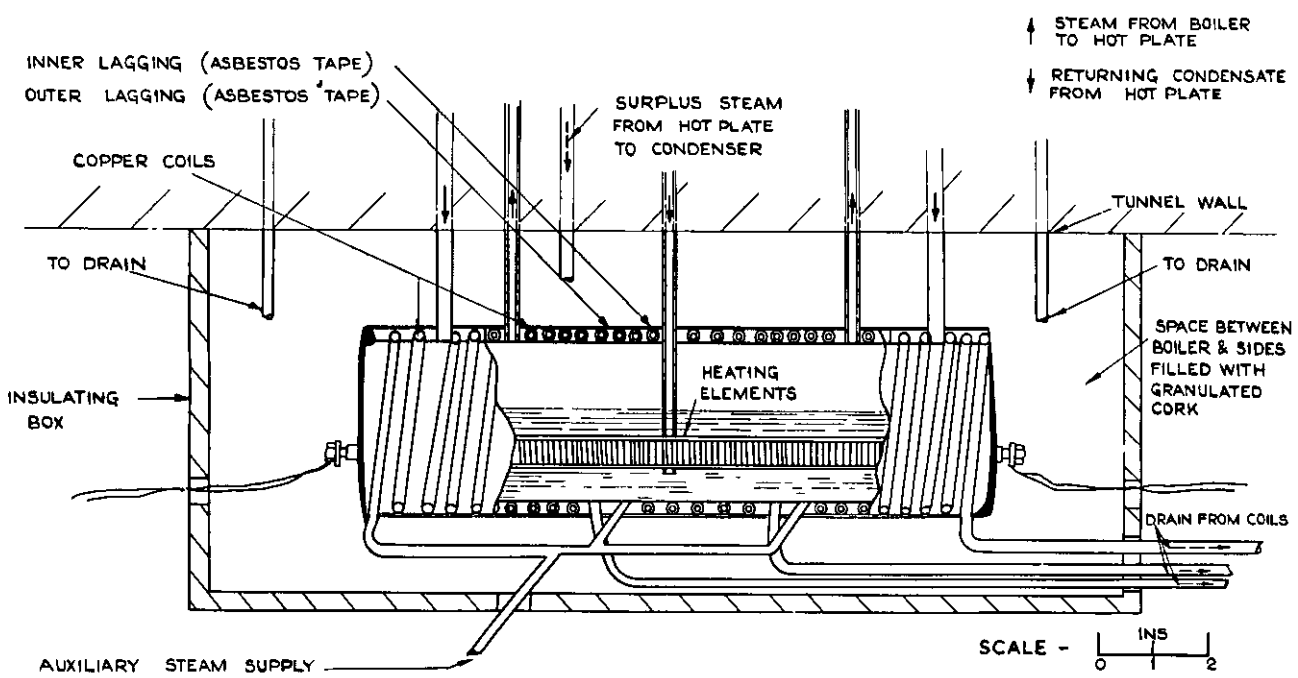

SECTION THROUGH BOX AND OUTER LAGGING AND PART SECTION THROUGH BOILER STEAM LAGGING SYSTEM.

FIG.I. GENERAL ARRANGEMENT OF TUNNEL.

FIG.2.

LETTERS & NUMBERS REFER TO MANOMETER BANK.

RINGED NUMBERS REFER TO SELECTOR SWITCH POSITIONS.

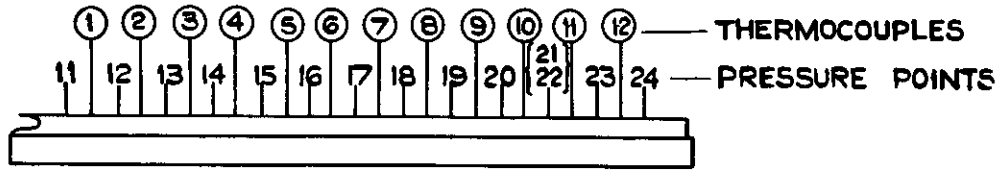

THERMOCOUPLES & PRESSURE POINTS ON PLATE.

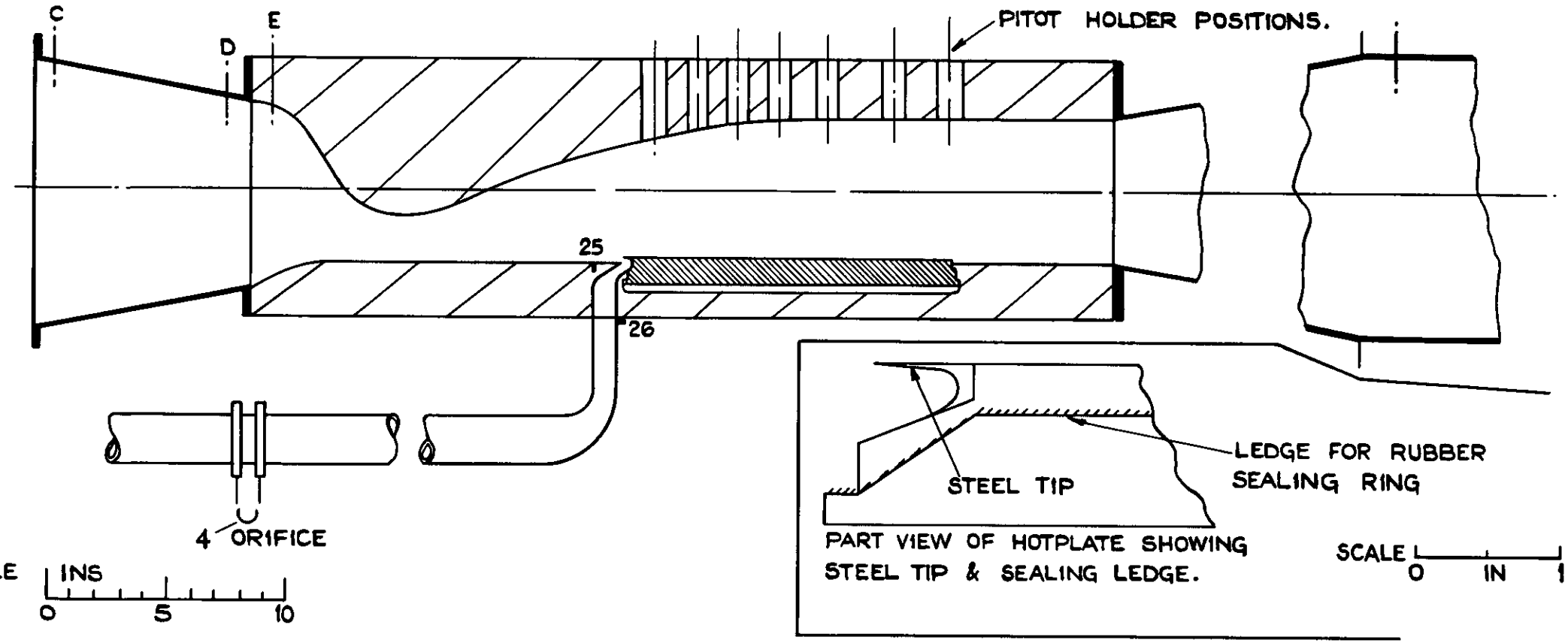

FIG. 2. LOCATION OF PRESSURE POINTS. THERMOCOUPLES & PITOT TRAVERSE HOLES.

FIG.3.

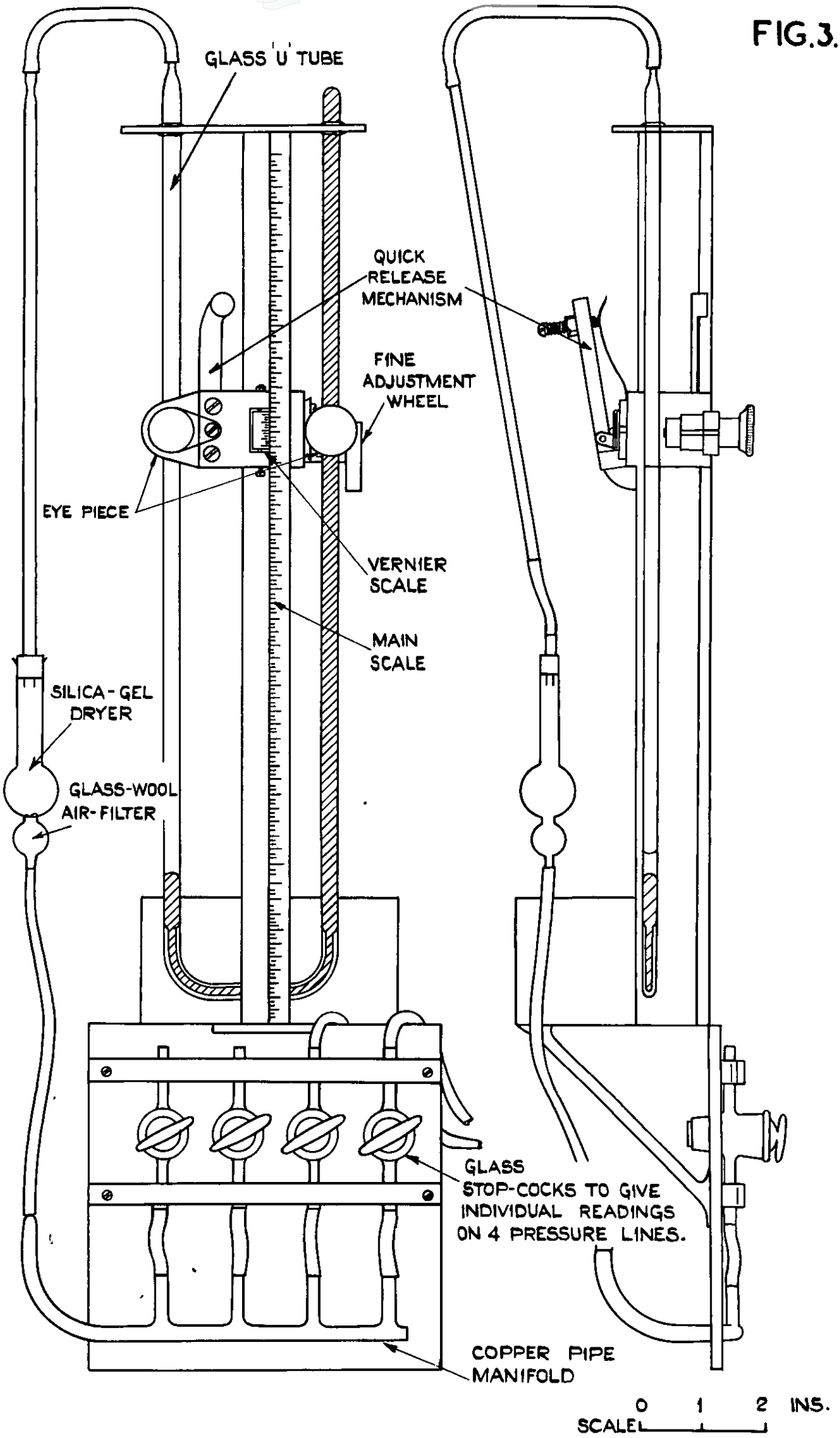

FIG. 3. ABSOLUTE MICRO-MANOMETER.

FIG. 4

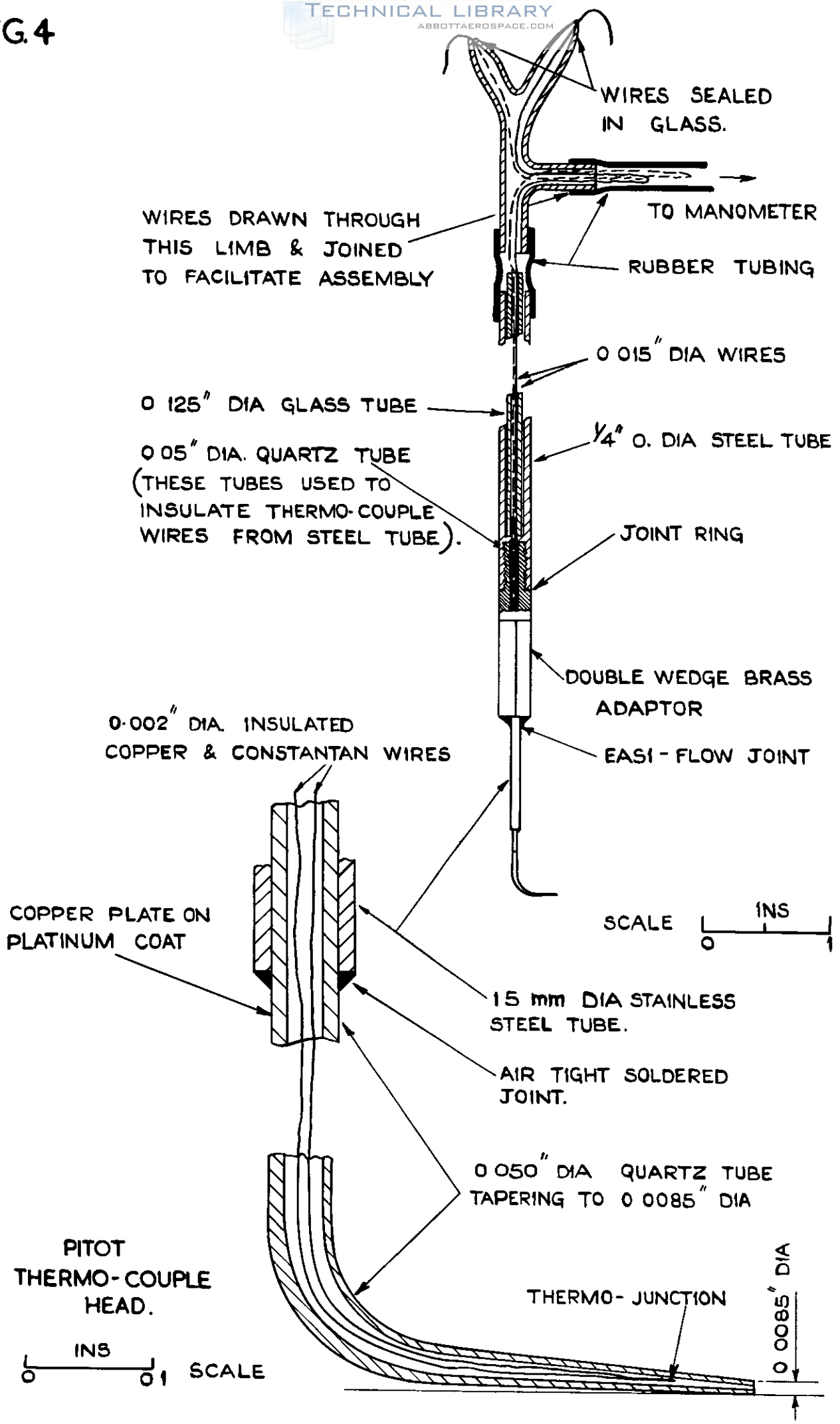

FIG. 4. TYPICAL TRAVERSING PITOT-THERMO-COUPLE.

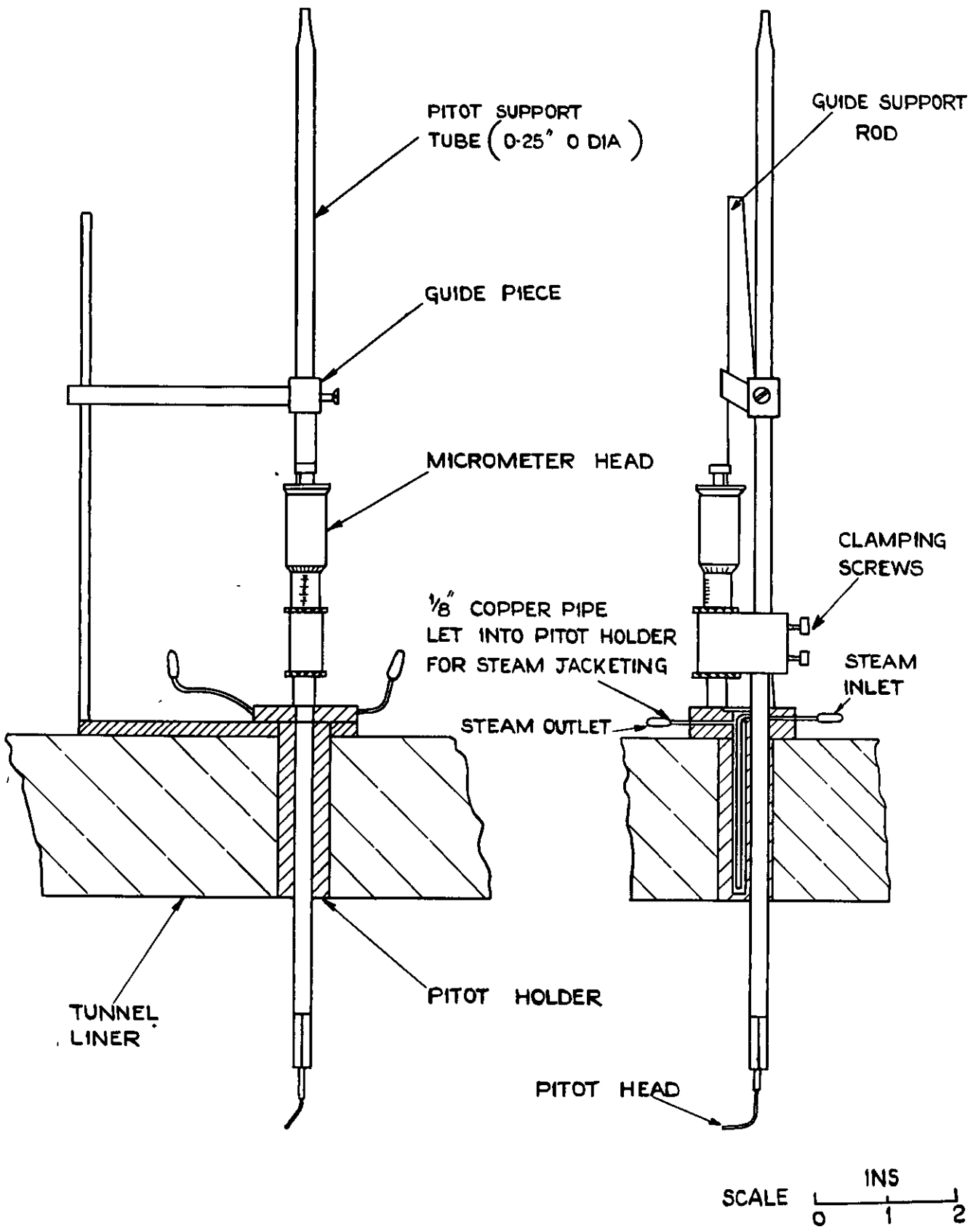

FIG. 5. DETAILS OF PITOT TUBE TRAVERSING GEAR.

FIG. 6.

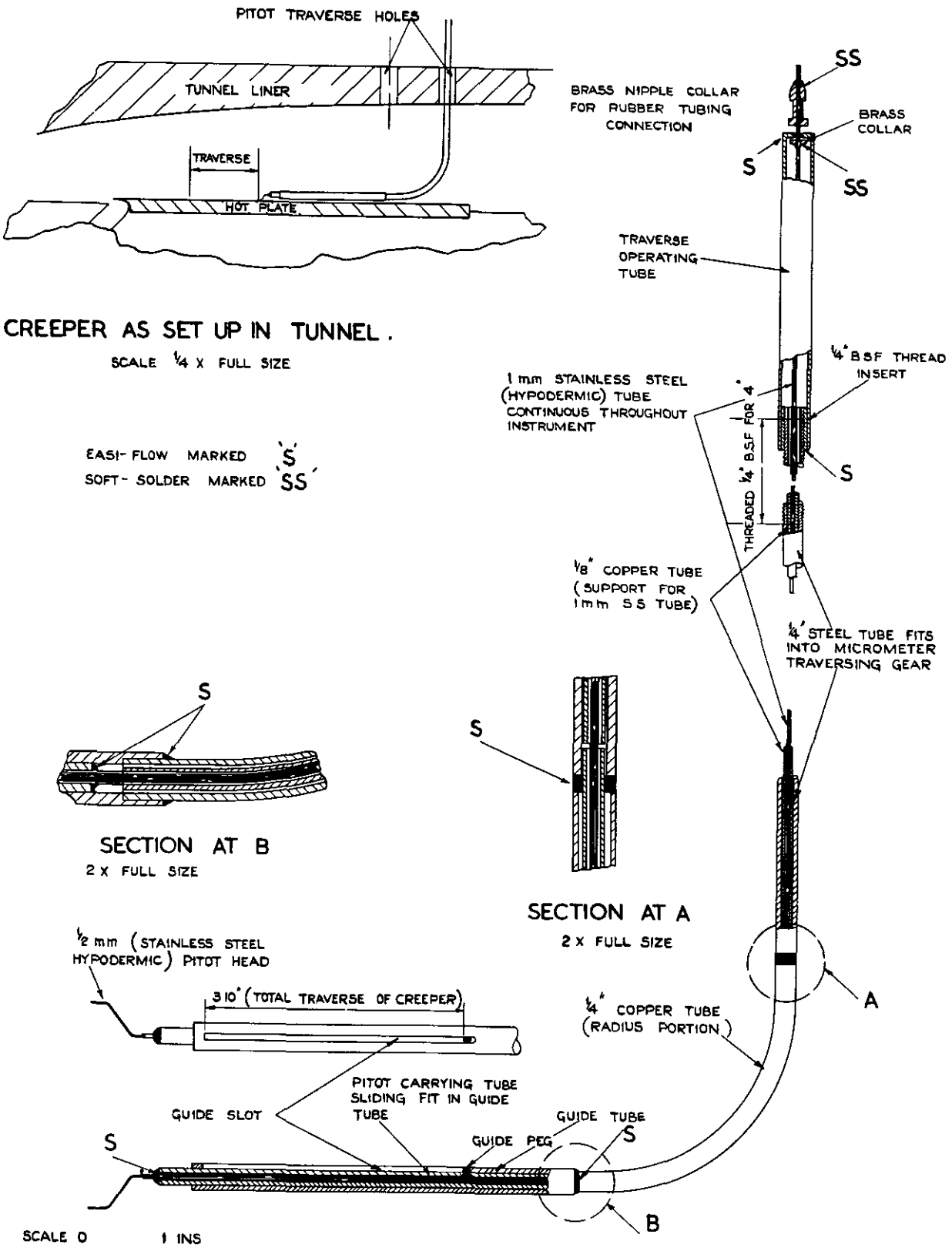

FIG. 6. TRANSITION INDICATION INSTRUMENT ("CREEPER")

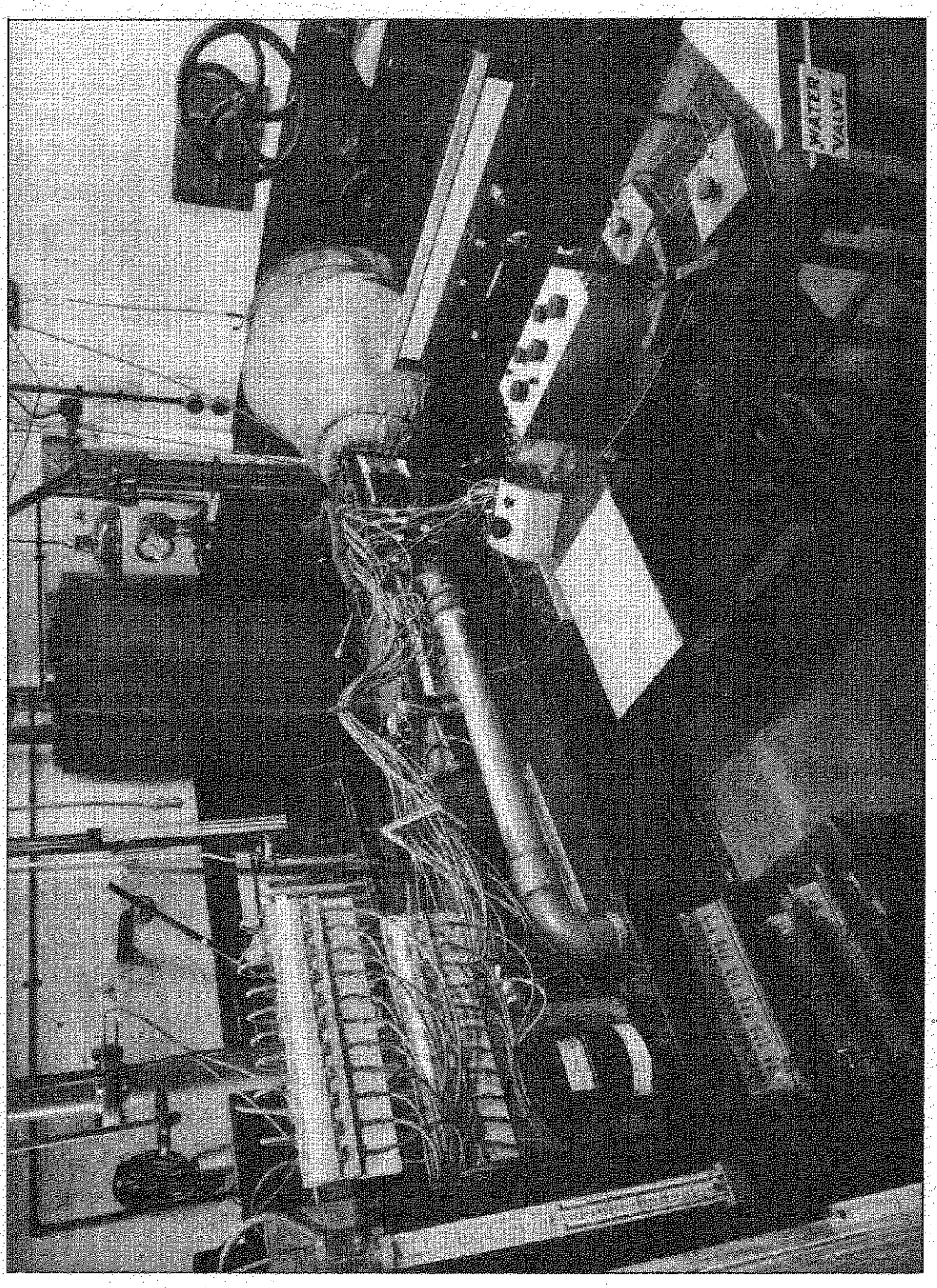

FIG.7a. GENERAL VIEW OF HOT-PLATE SIDE OF TUNNEL SHOWING TEMPERATURE MEASURING EQUIPMENT

FIG.7b

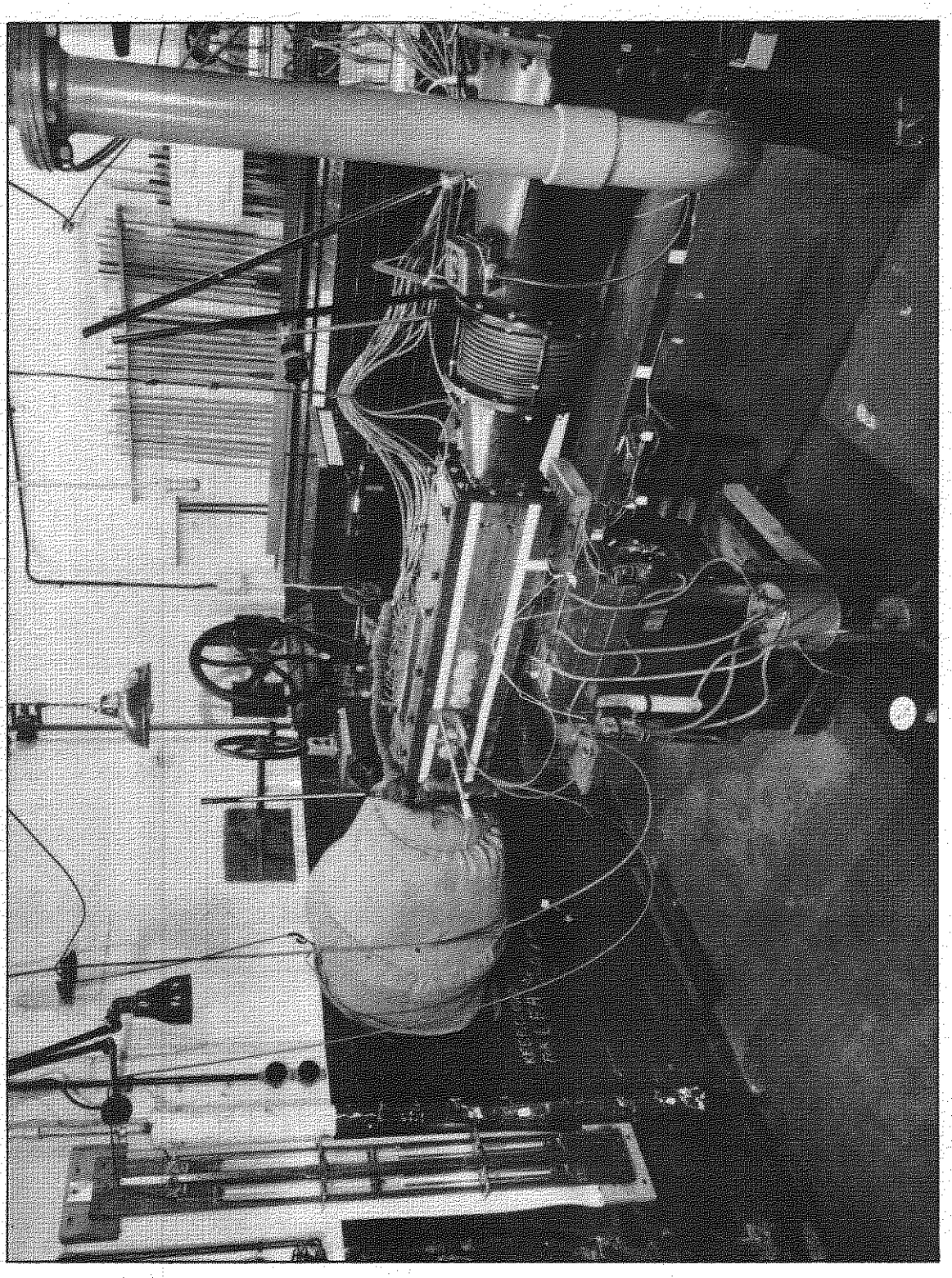

FIG.7b. GENERAL VIEW OF PITOT HOLDER, MANOMETER AND CONNECTIONS FOR HEATING PLATE BY PROCESS STEAM

FIG. 8(a & b)

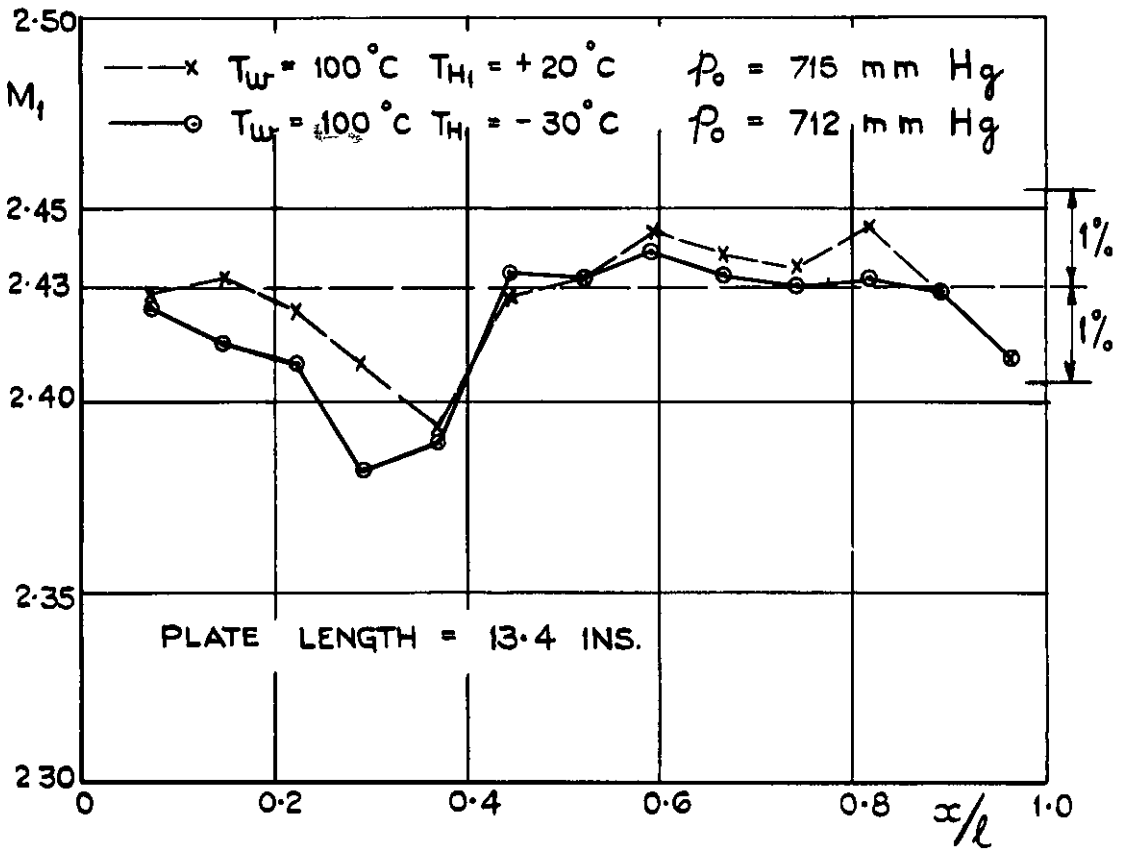

(a) DURING HEAT TRANSFER TESTS.

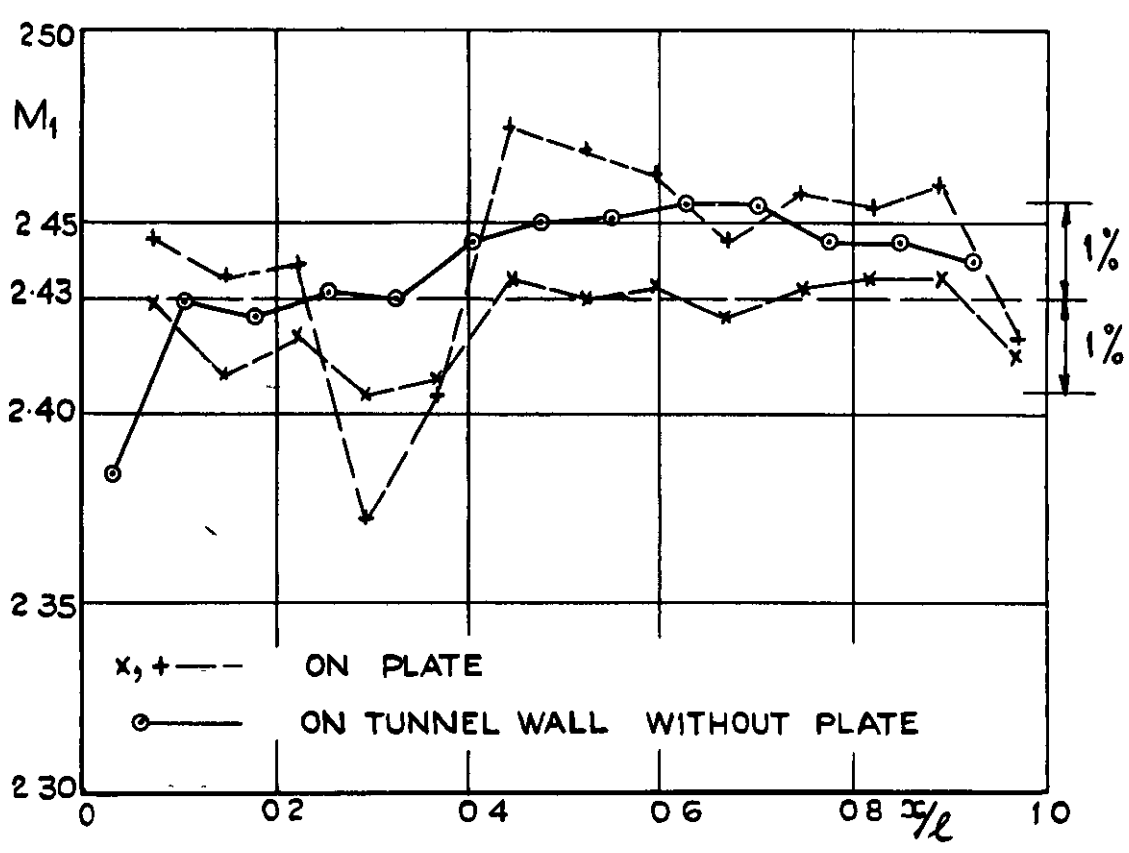

(b) DURING ZERO HEAT TRANSFER TESTS.

FIG. 8. (a & b) MACH NUMBER DISTRIBUTIONS ALONG PLATE.

FIG. 9(a & b)

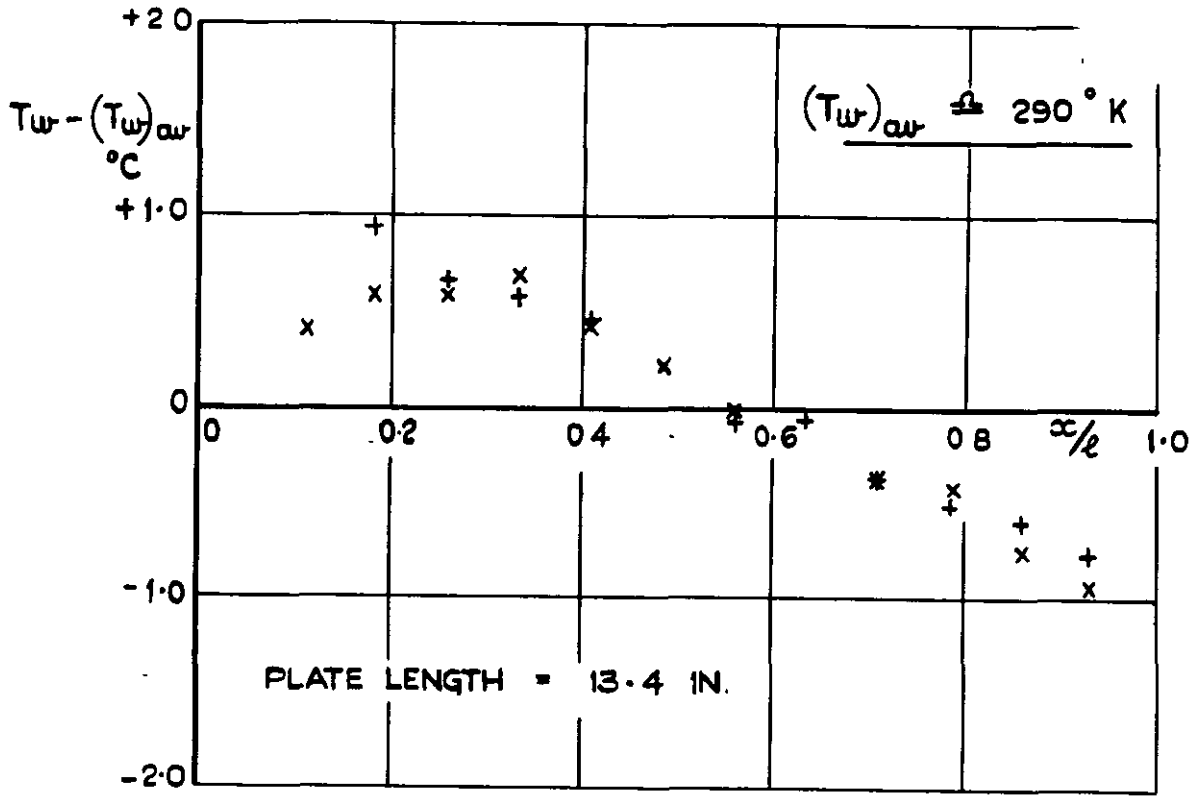

(a) DURING ZERO HEAT TRANSFER TESTS.

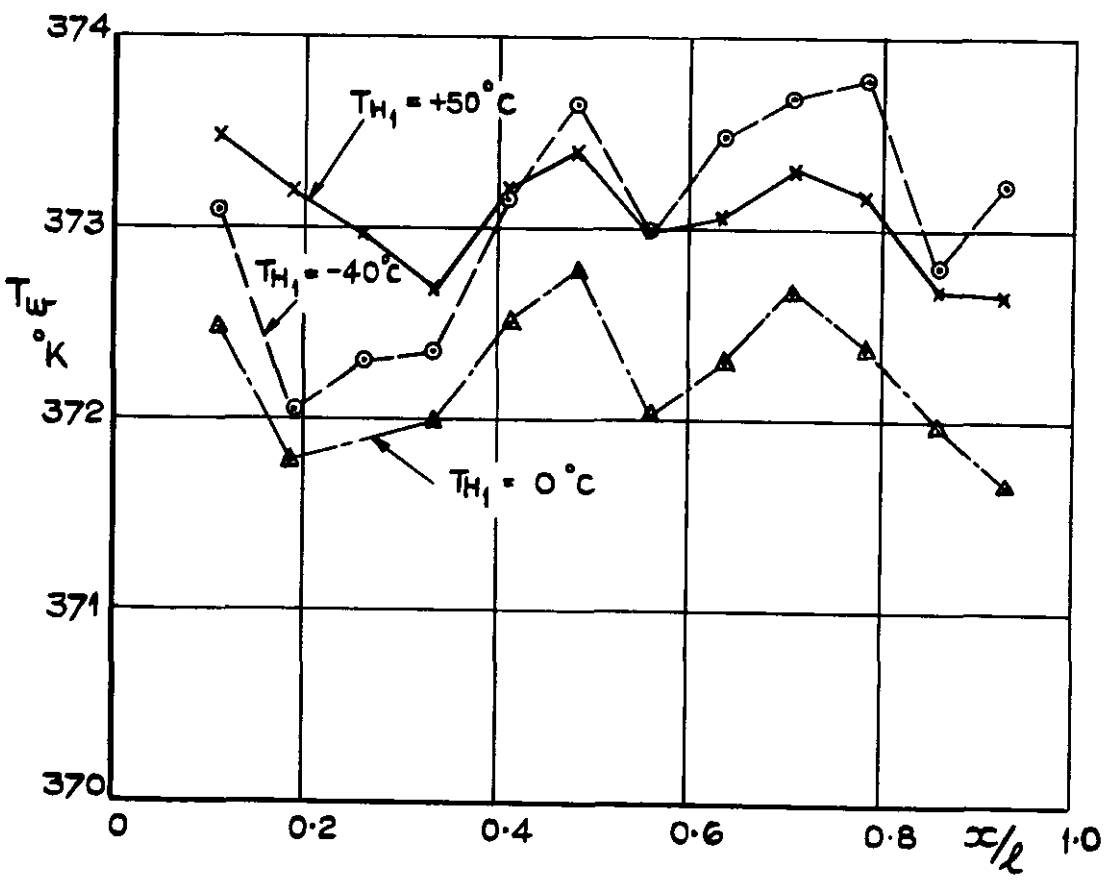

(b) DURING HEAT TRANSFER TESTS.

FIG. 9(a&b) TYPICAL SURFACE TEMPERATURE DISTRIBUTIONS ON PLATE.
$M_1 = 2·43$.

FIG. 10.

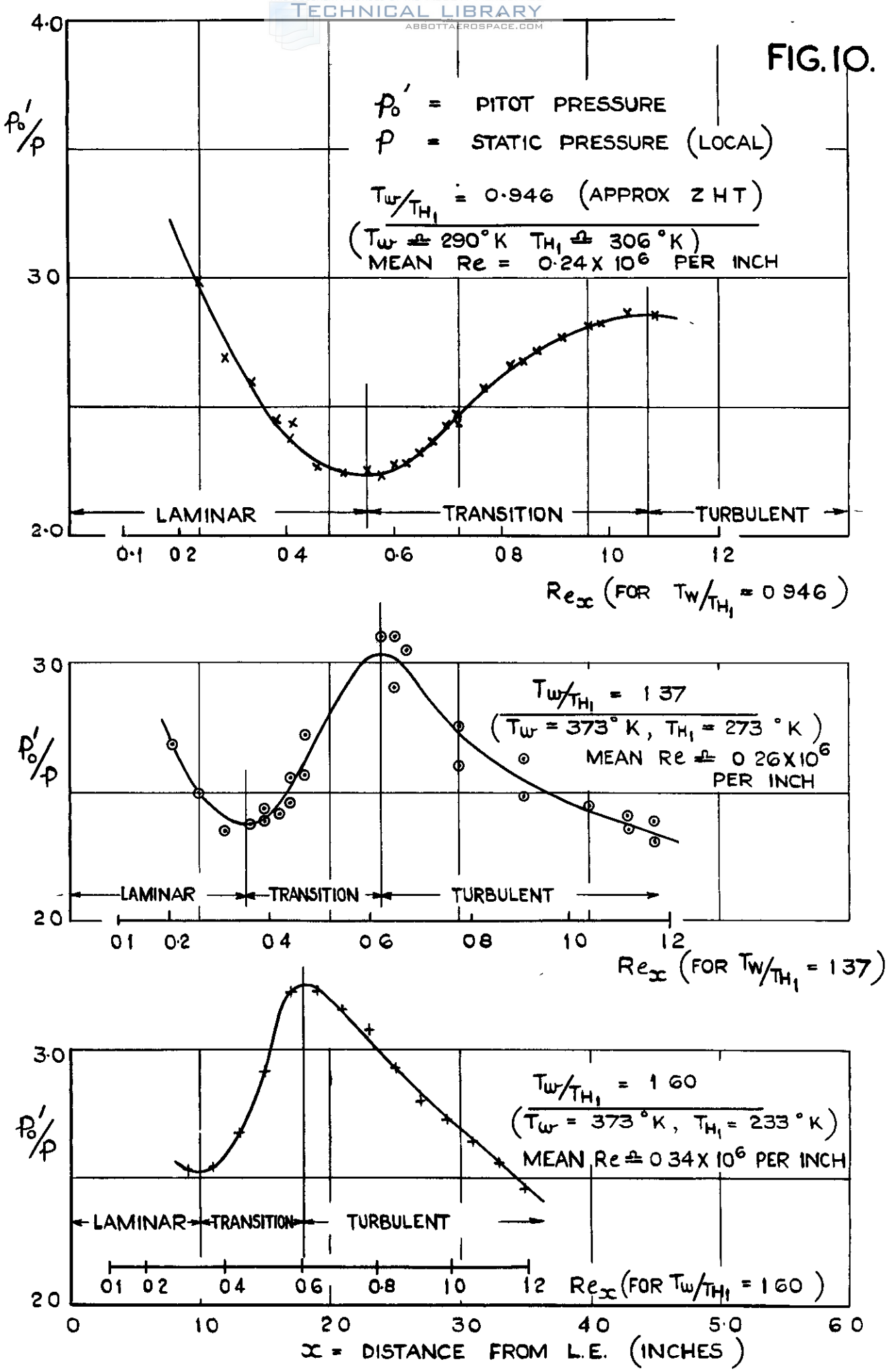

FIG. 10. MOVEMENT OF BOUNDARY LAYER TRANSITION WITH HEAT TRANSFER.

(TRAVERSES ALONG PLATE CENTRE LINE. M_1 = 2·43)

FIG. II.

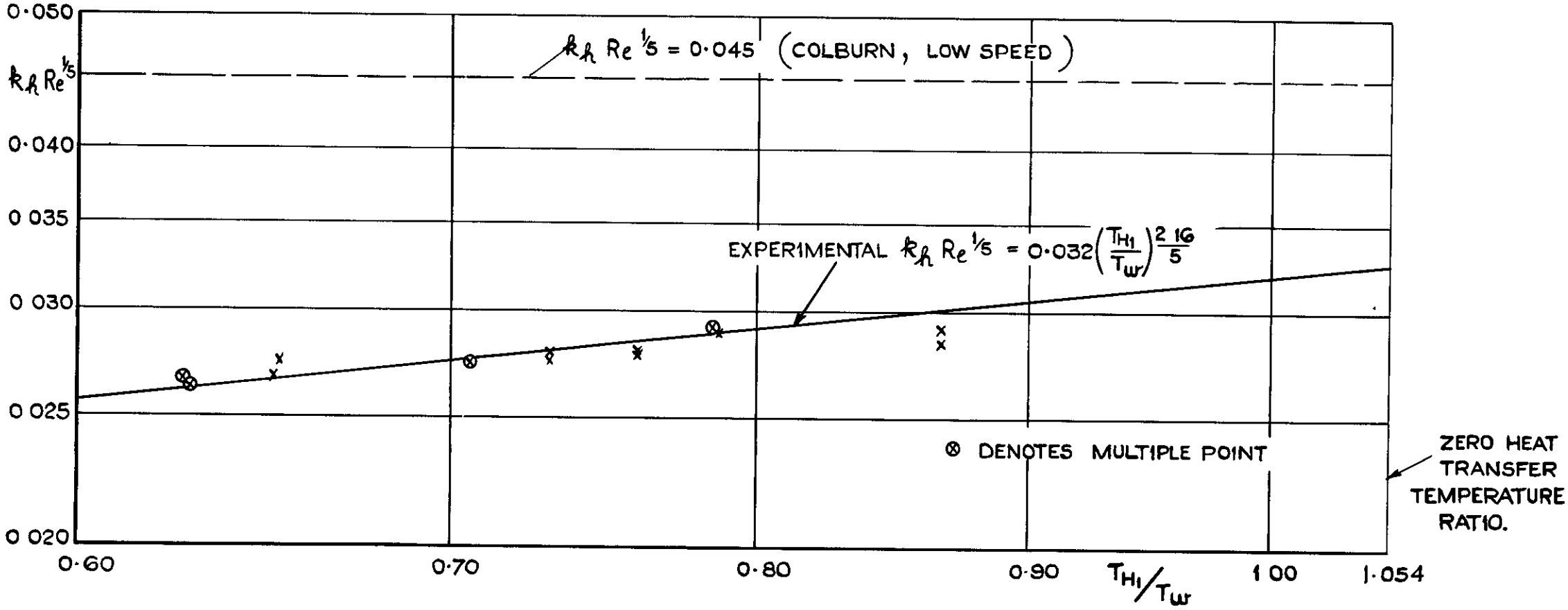

FIG. II. VARIATION OF OVERALL HEAT TRANSFER COEFFICIENT WITH TEMPERATURE

$M_1 = 2{\cdot}43$ T_w 373° K

$$k_h = \frac{Q/S}{\rho_1 u_1 g C_p (T_w - T_{w0})} \qquad Re = \frac{u_1 l}{\nu_1}$$

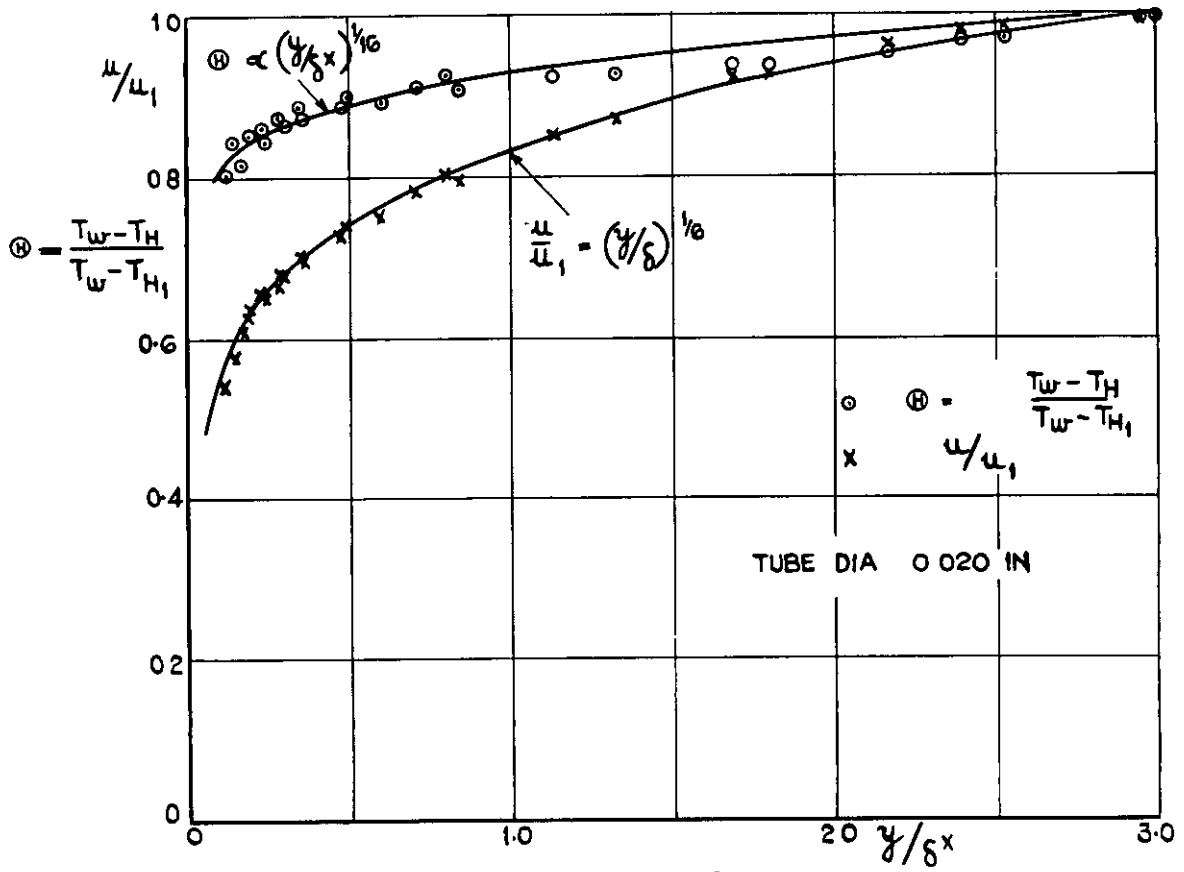

(a) $T_w/T_{H_1} = 1.35$ $T_w = 373\ ^\circ K.$ $T_{H_1} = 276.5\ ^\circ K.$

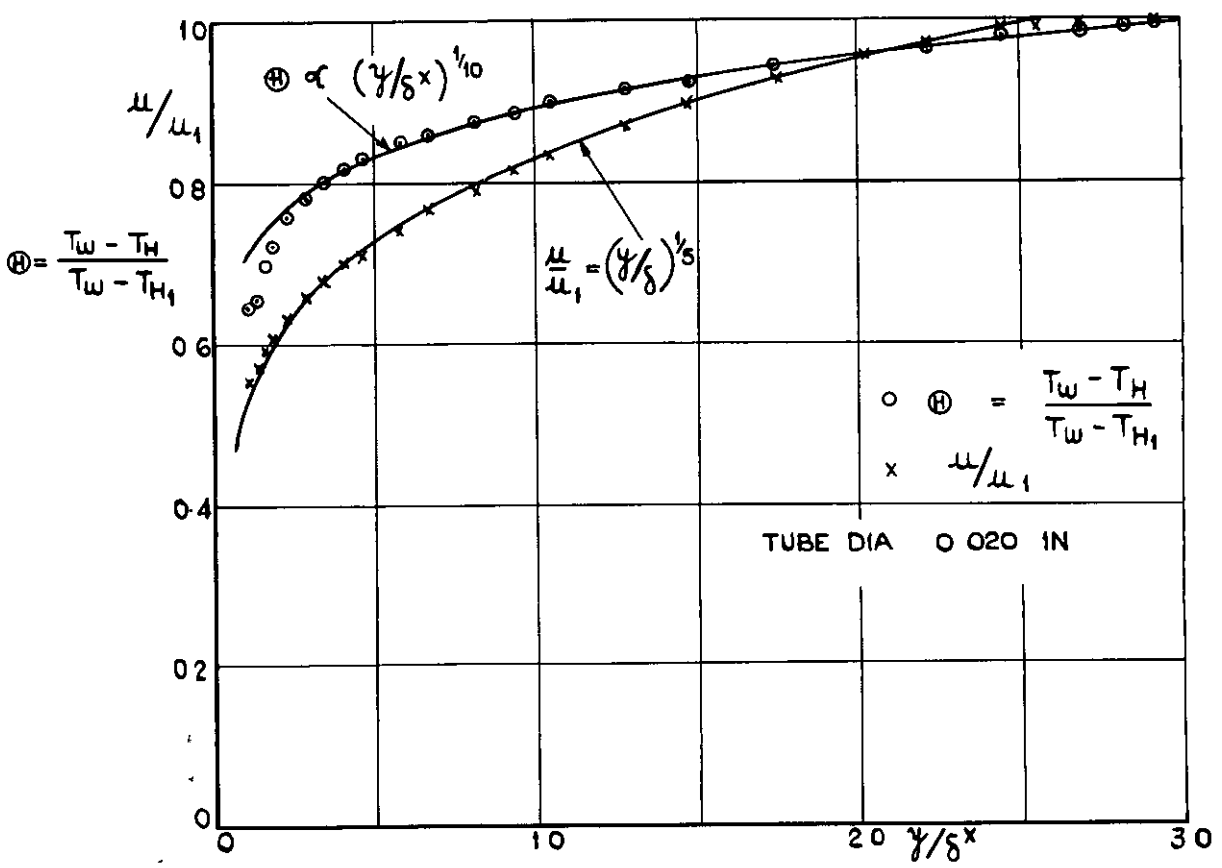

(b) $T_w/T_{H_1} = 1.57$ $T_w = 373\ ^\circ K$ $T_{H_1} = 237\ ^\circ K.$

FIG. 12.(a & b) TEMPERATURE & VELOCITY DISTRIBUTIONS. IN BOUNDARY LAYER. $M_1 = 2.43.$

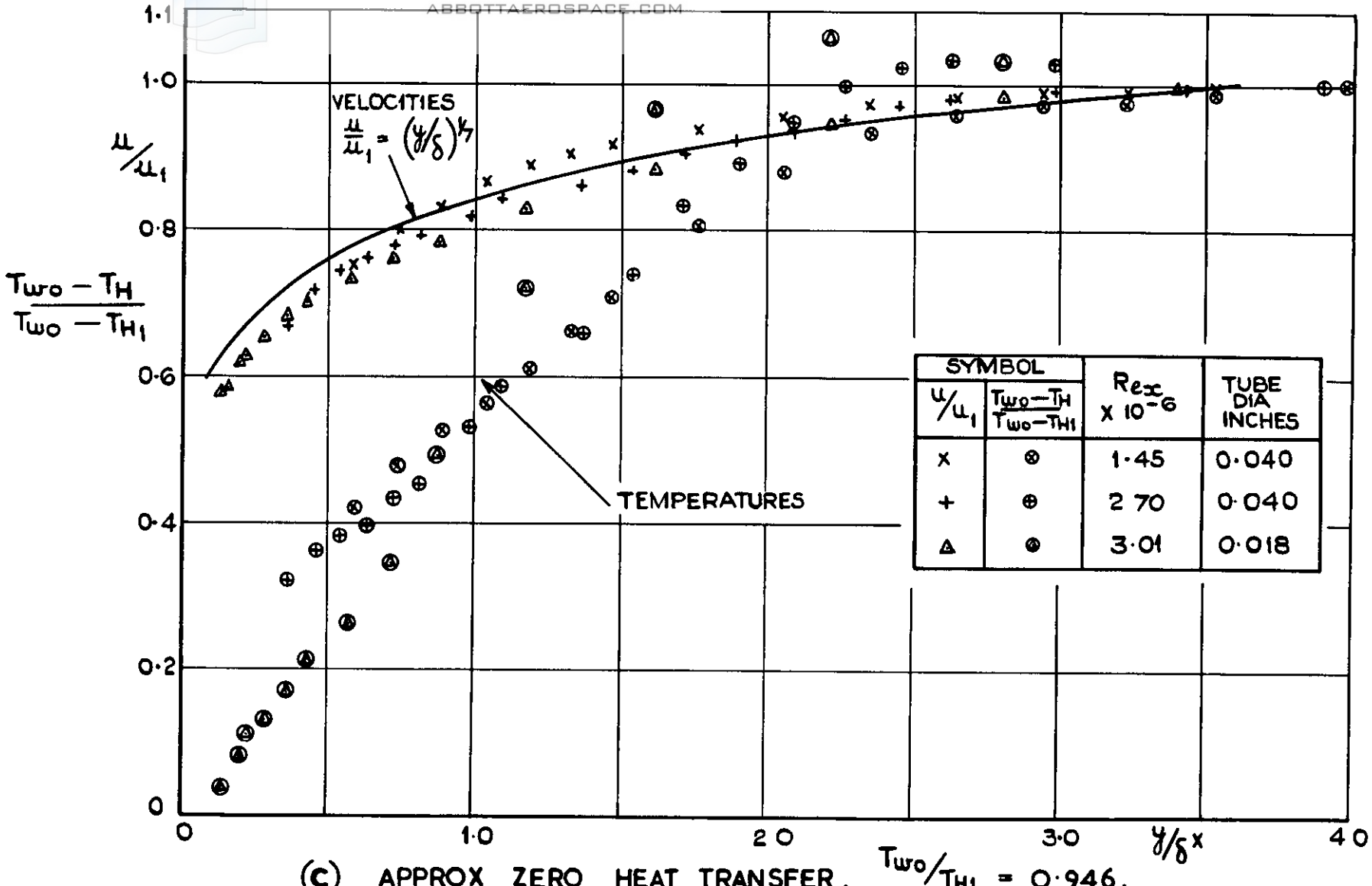

(c) APPROX ZERO HEAT TRANSFER.

FIG. 12. (c.) TEMPERATURE AND VELOCITY DISTRIBUTIONS IN BOUNDARY LAYER. $M_1 = 2·43$

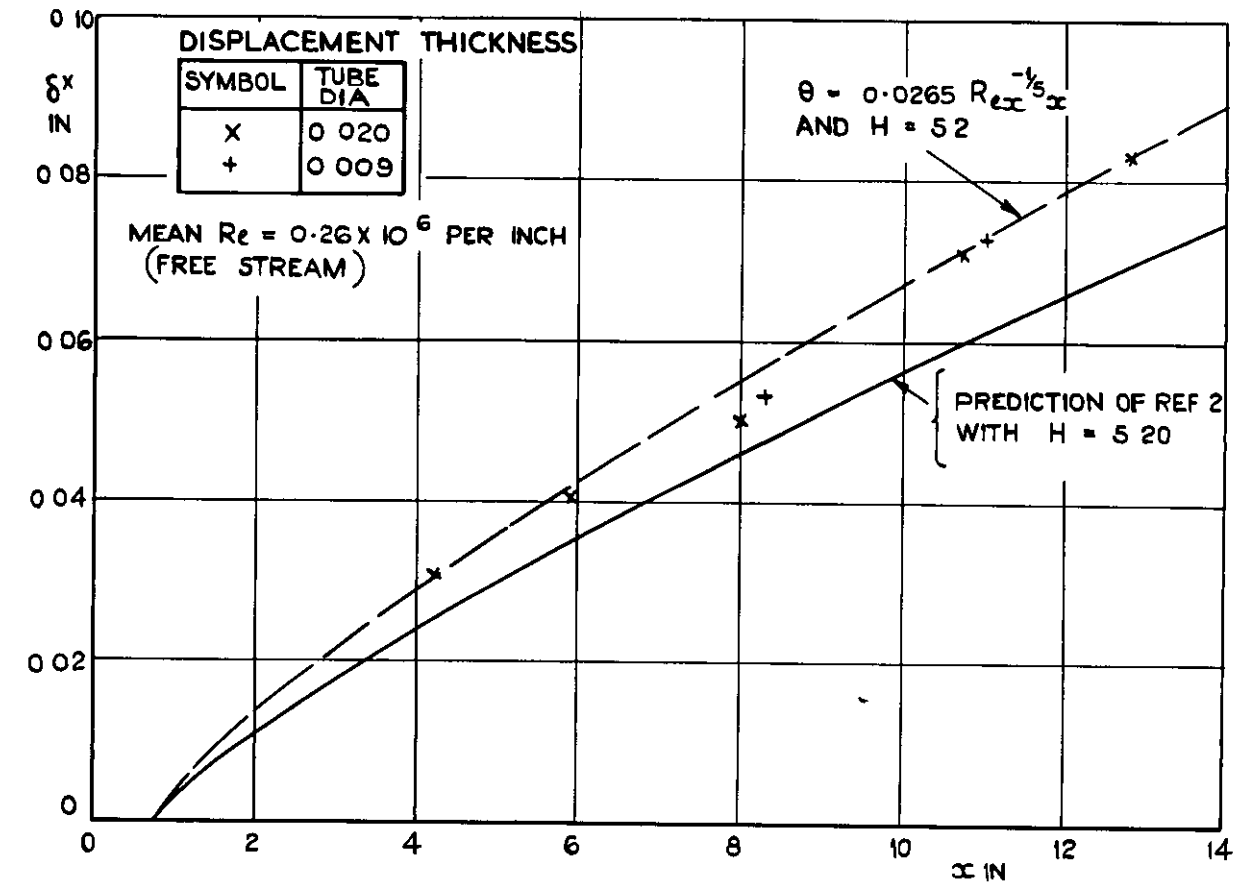

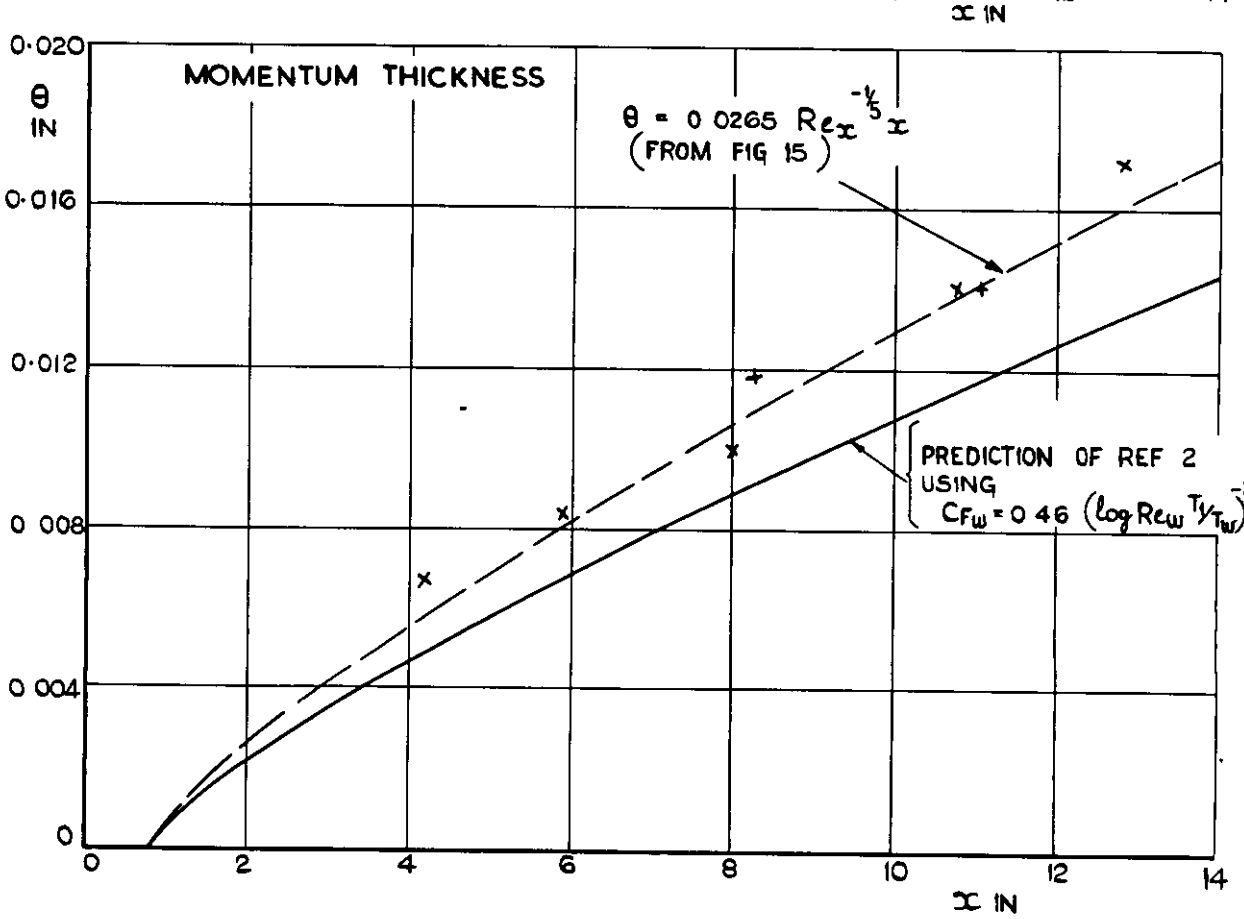

FIG. 13. DISPLACEMENT AND MOMENTUM THICKNESSES

T_w = 373 °K T_{H_1} = 276·5 °K.

FIG. 14.

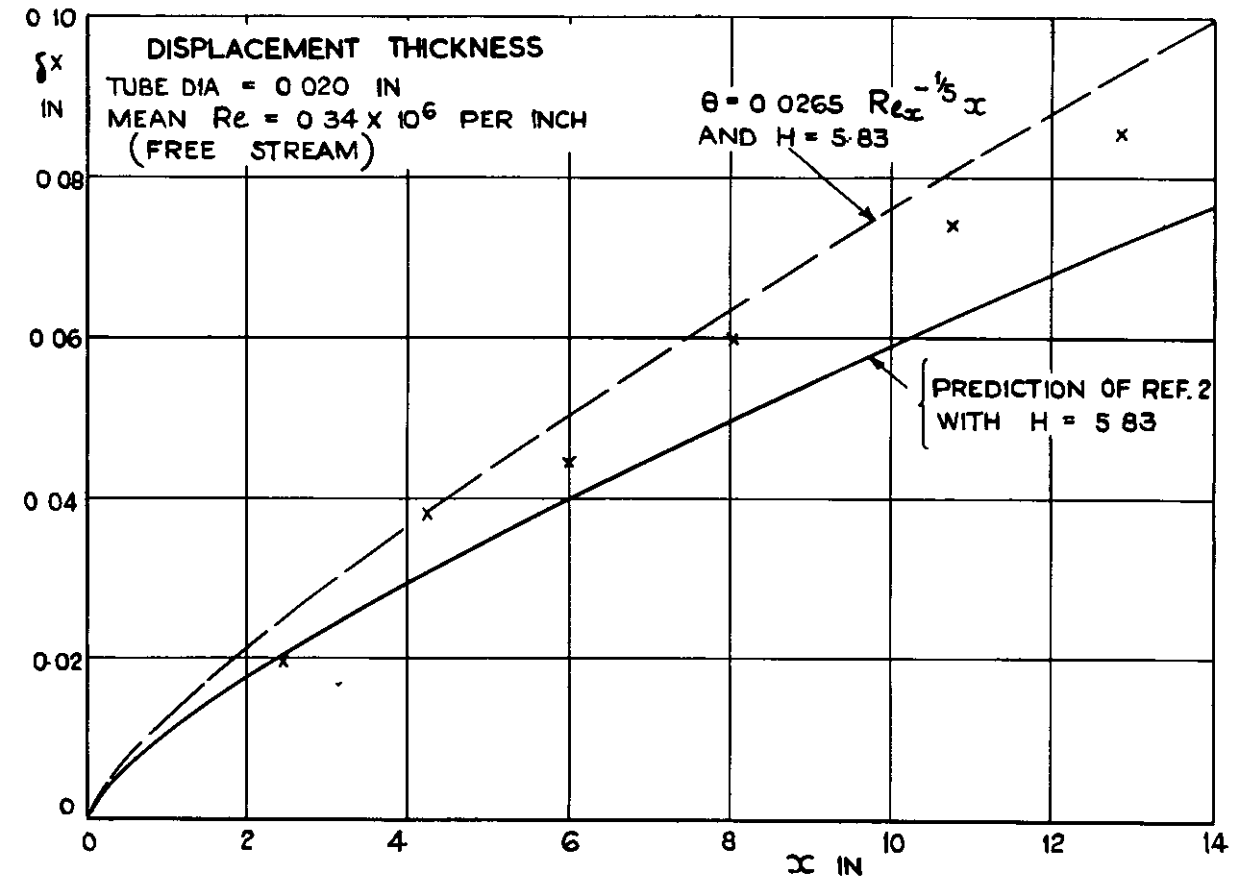

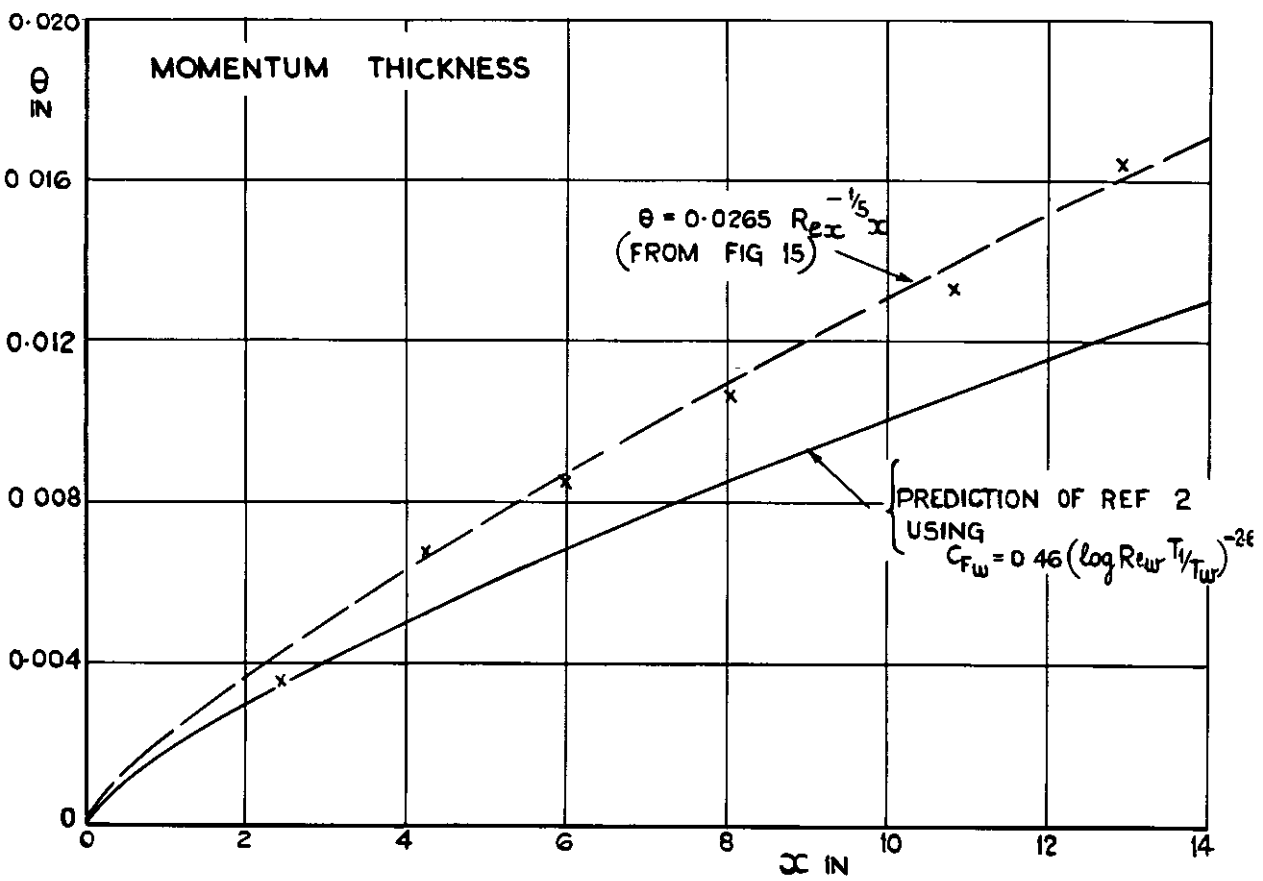

FIG. 14. DISPLACEMENT AND MOMENTUM THICKNESSES
T_w = 373° K. T_{H_1} 237 °K

FIG. 15.

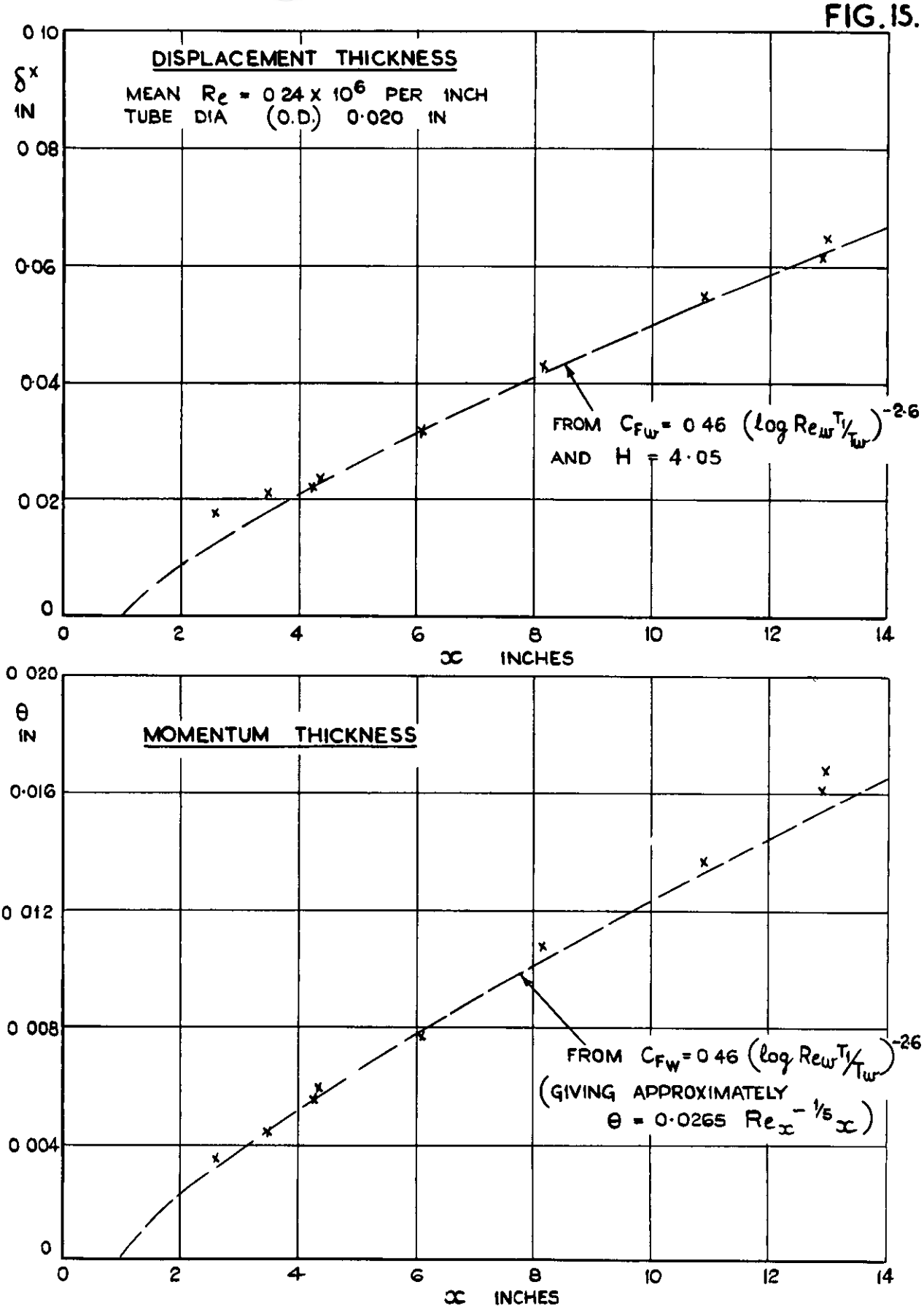

FIG. 15. DISPLACEMENT AND MOMENTUM THICKNESSES
ZERO HEAT TRANSFER $(T_{wo}/T_1 = 2.06)$
(TAKEN FROM REF. 2)

FIG. 16.

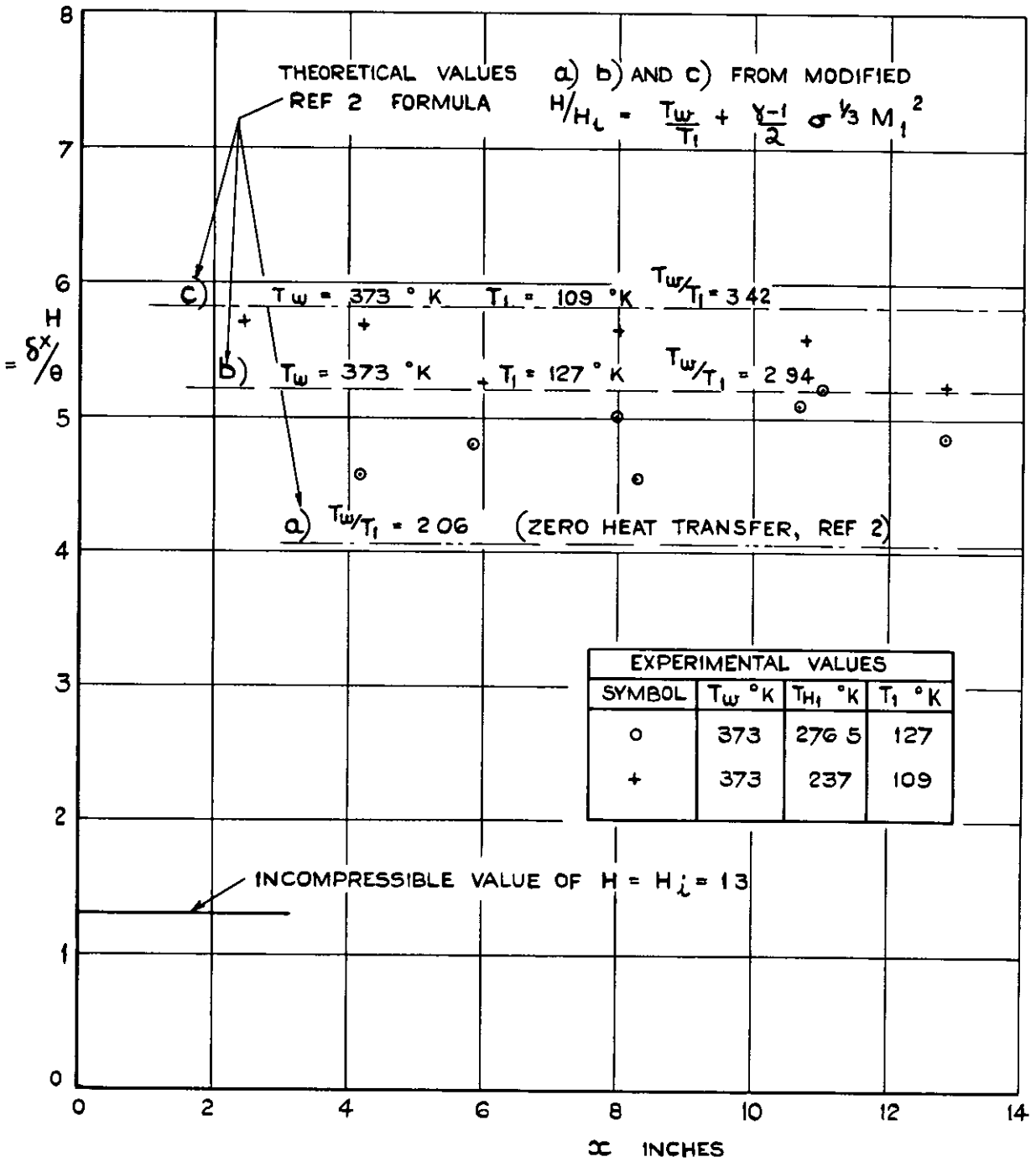

FIG. 16. RATIO OF DISPLACEMENT TO MOMENTUM THICKNESS.

(TURBULENT BOUNDARY LAYER, $M_1 = 2 \cdot 43$.)

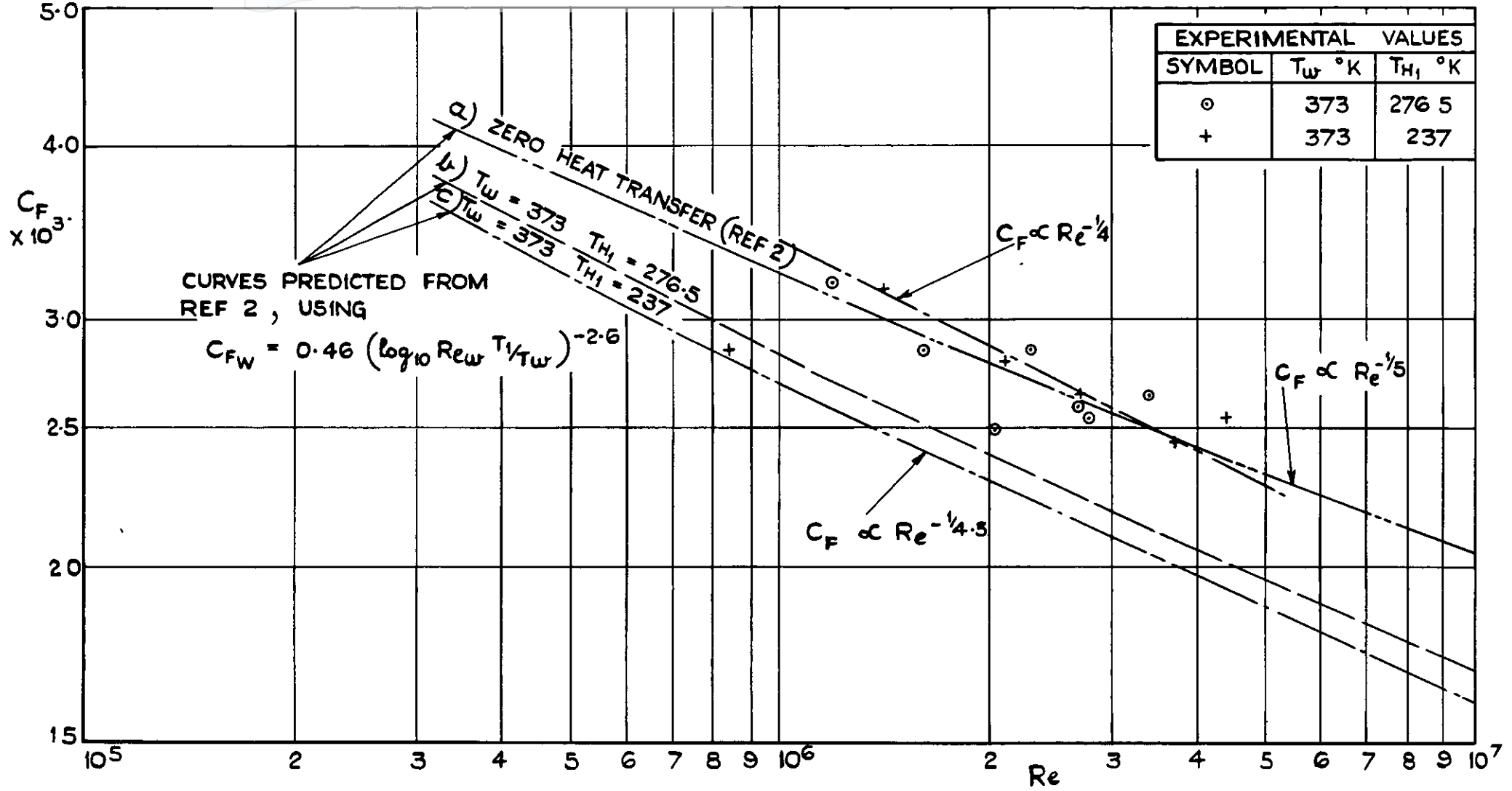

FIG. 17. VARIATION OF SKIN FRICTION COEFFICIENT WITH REYNOLDS NUMBER UNDER HEAT TRANSFER CONDITIONS AT $M_1 = 2 \cdot 43$.

$$C_F = \frac{F}{\frac{1}{2} \rho_1 \mu_1^2 x} \qquad Re = \frac{\mu_1 x}{\nu_1}$$

FIG.17.

FIG.18.

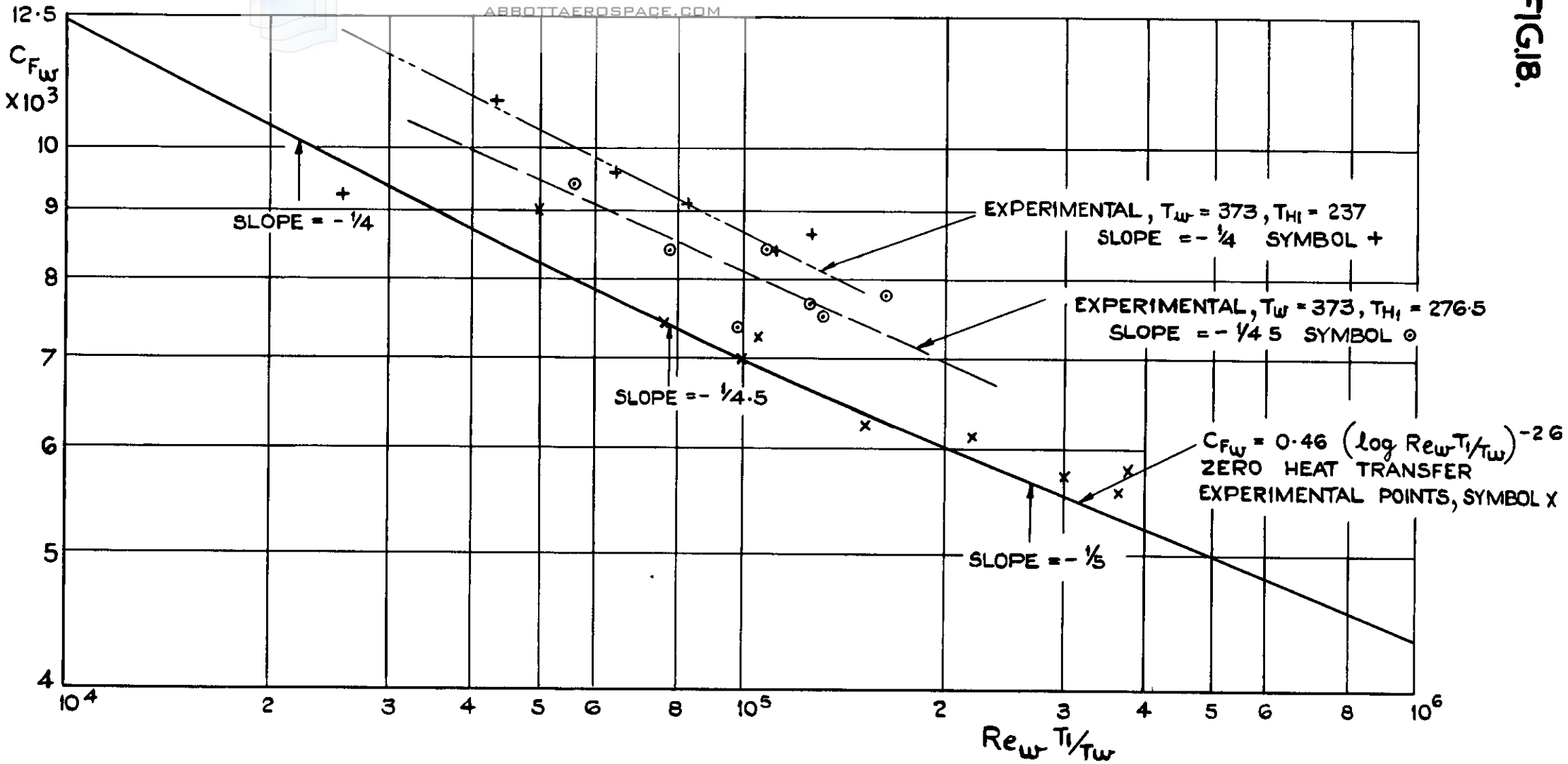

FIG. 18. VARIATION OF C_{F_w} WITH $Re_w \; T_1/T_w$ UNDER HEAT TRANSFER CONDITIONS.

$$C_{F_w} = \frac{F}{\frac{1}{2} \rho_w u_1^2 x} \qquad Re_w \, T_1/T_w = \frac{u_1 x}{\nu_w} \quad \frac{T_1}{T_w}$$

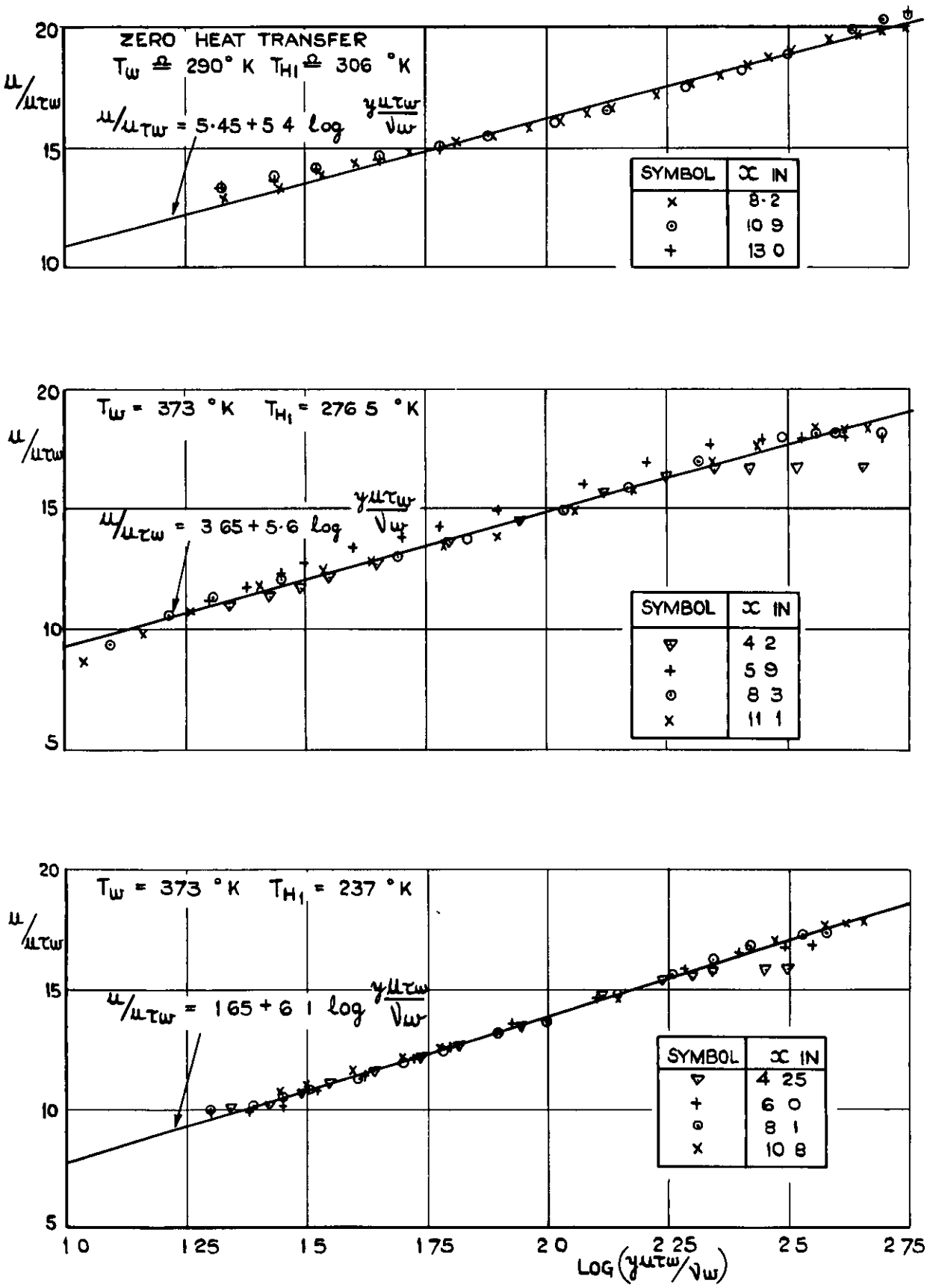

FIG. 19. VELOCITY DISTRIBUTIONS (LOG LAW) $M_1 = 2.43$ (LOCAL SKIN FRICTION ESTIMATED FROM FIGS. 13–15)

FIG. 20.

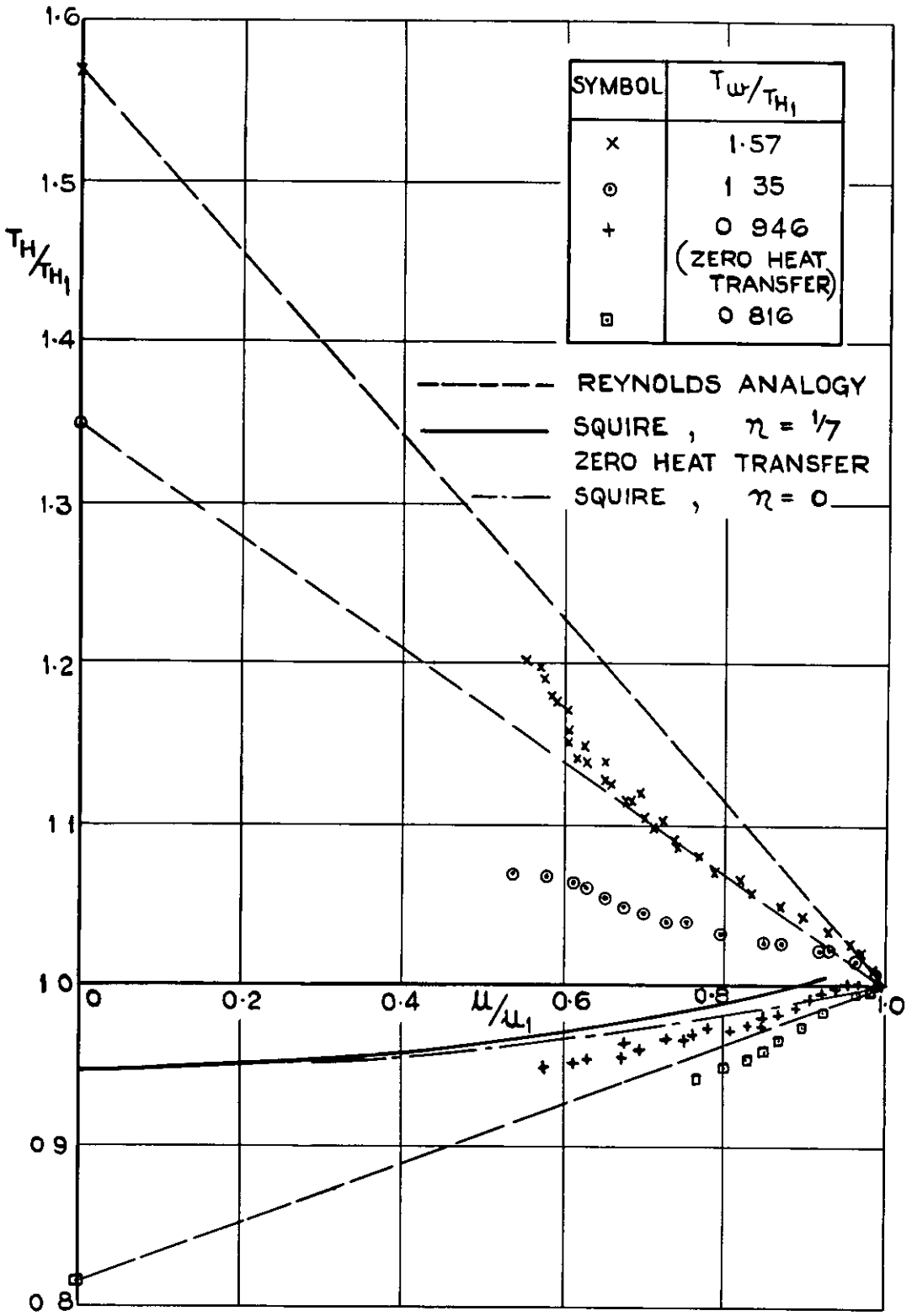

FIG. 20. (TOTAL TEMPERATURE)—VELOCITY DISTRIBUTIONS IN TURBULENT BOUNDARY LAYER $M_1 = 2 \cdot 43$.

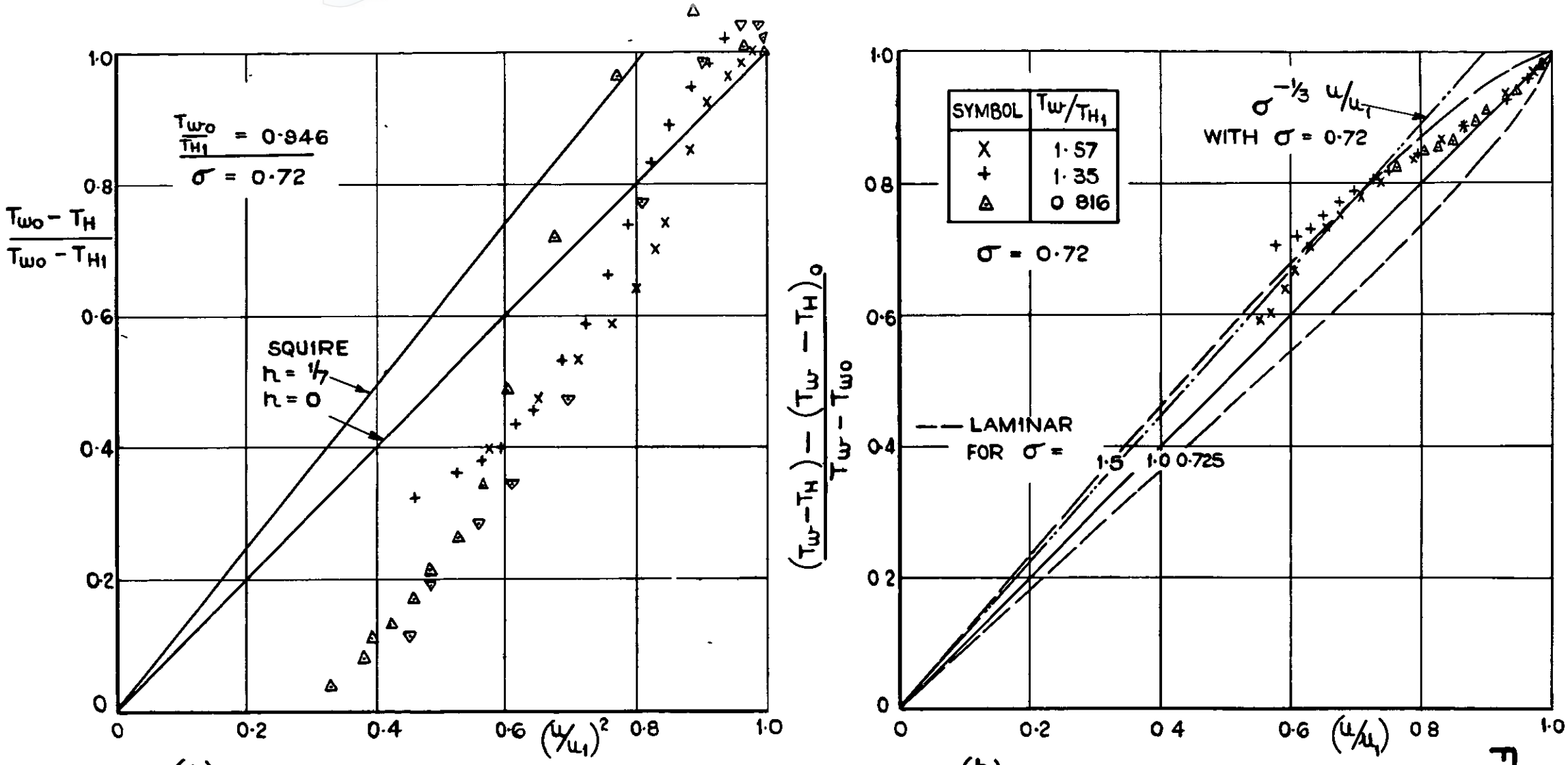

FIG. 21(a & b) COLLAPSED TOTAL TEMPERATURE—VELOCITY DISTRIBUTIONS.
$M_1 = 2.43$.

FIG21(a & b)

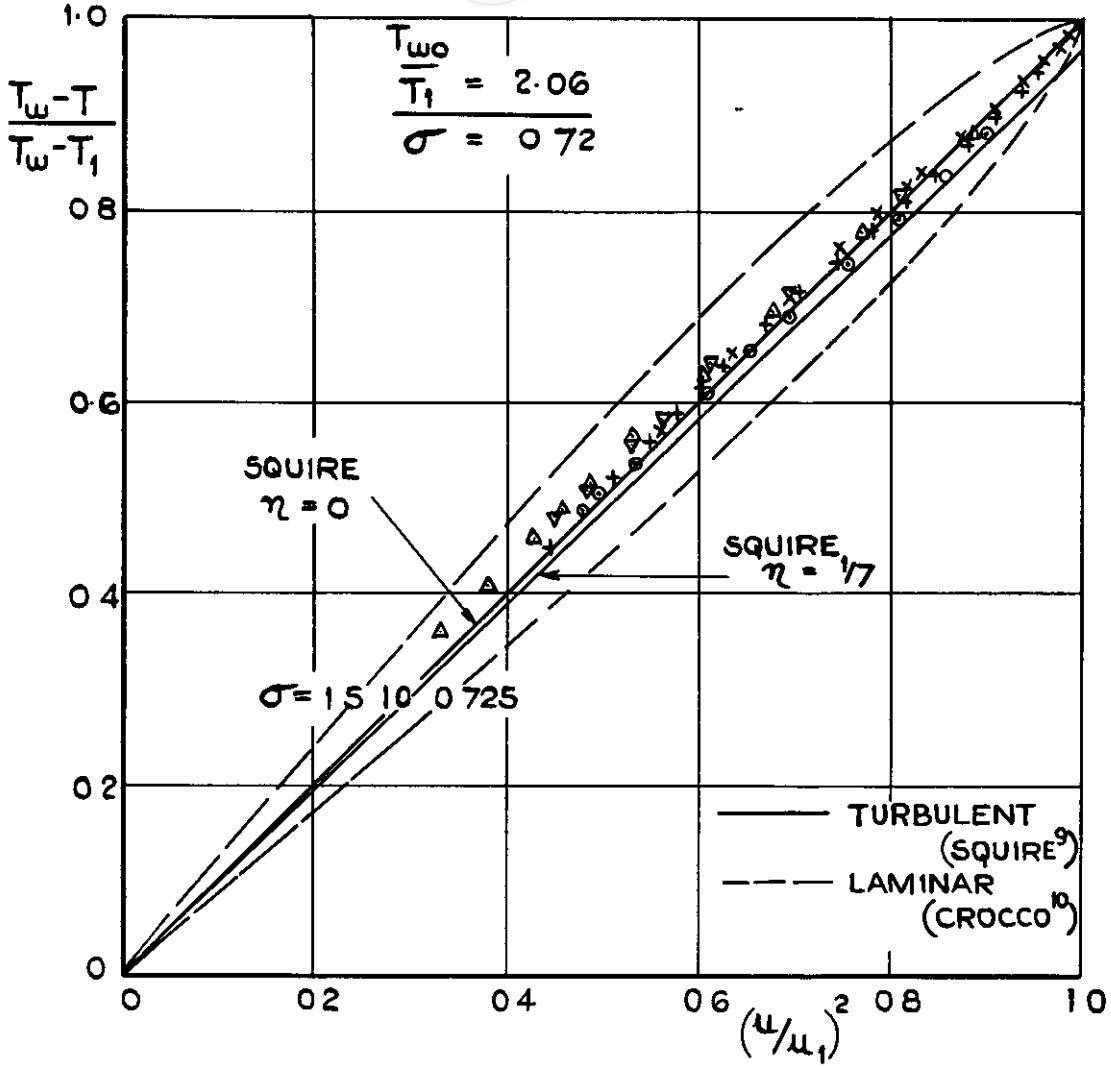

(a) ZERO HEAT TRANSFER.

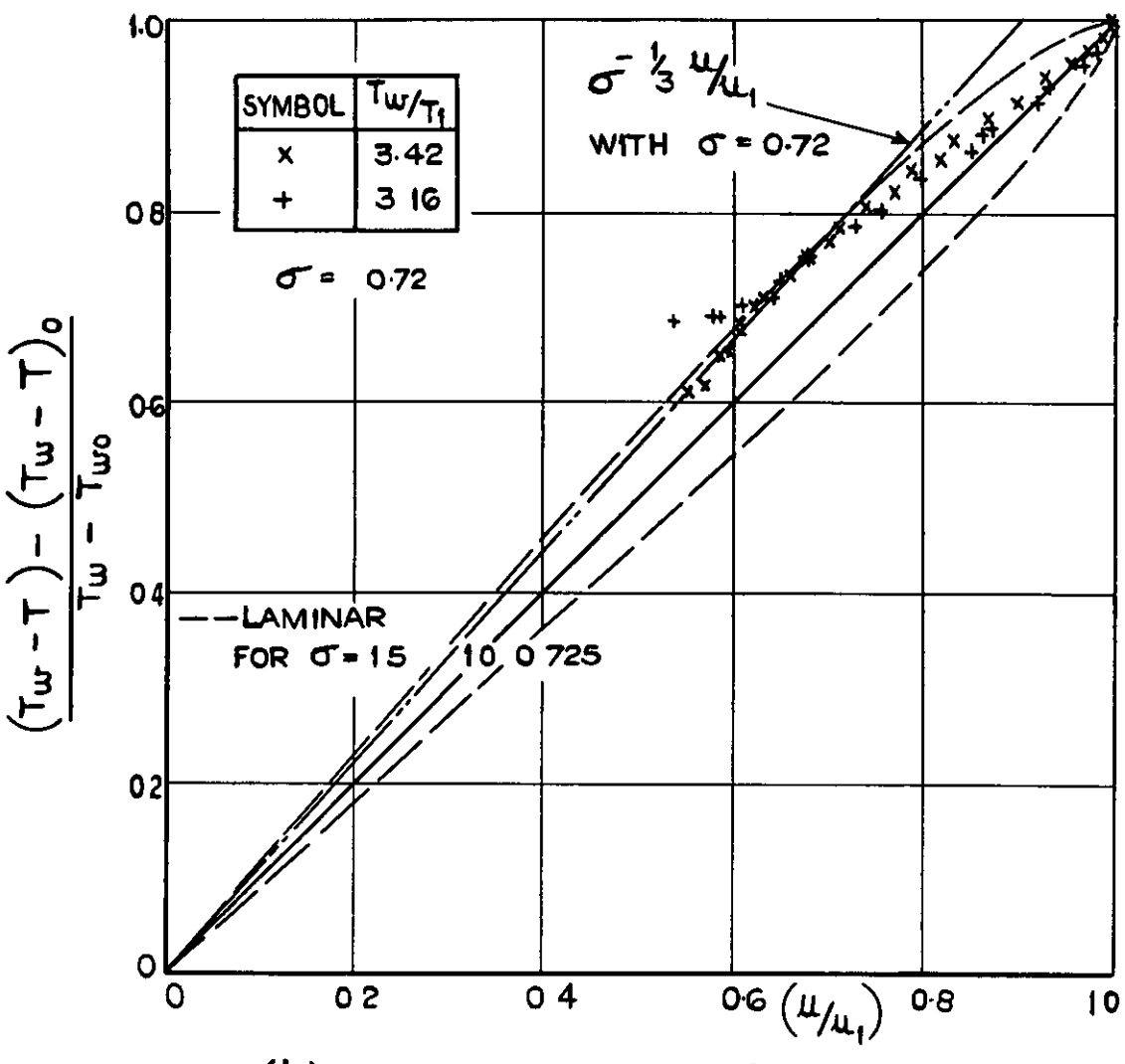

(b) WITH HEAT TRANSFER.

FIG. 22 (a & b) COLLAPSED STATIC TEMPERATURE-VELOCITY DISTRIBUTIONS.
$M_1 = 2.43$

FIG. 22(a & b)

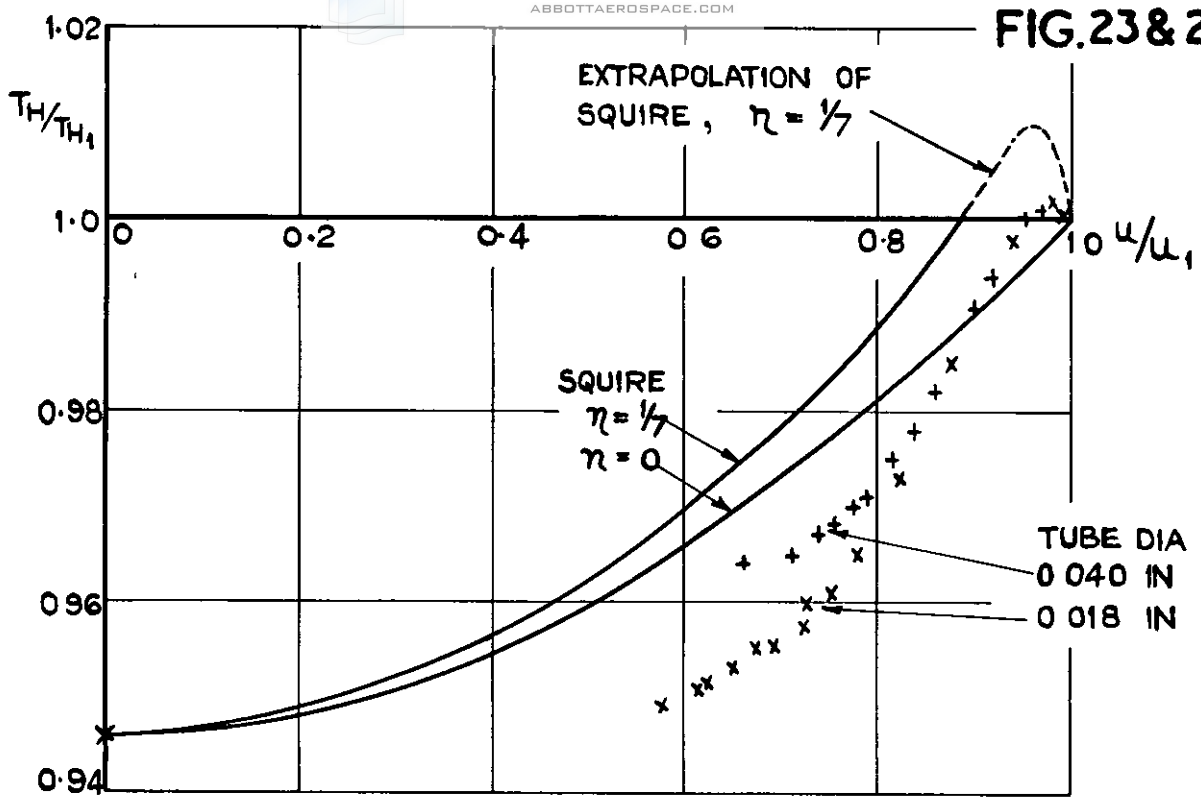

FIG. 23. TOTAL TEMPERATURE-VELOCITY DISTRIBUTION ZERO HEAT TRANSFER $T_{H_1} \triangleq 306$ °K (ENLARGED FROM FIG. 20.)

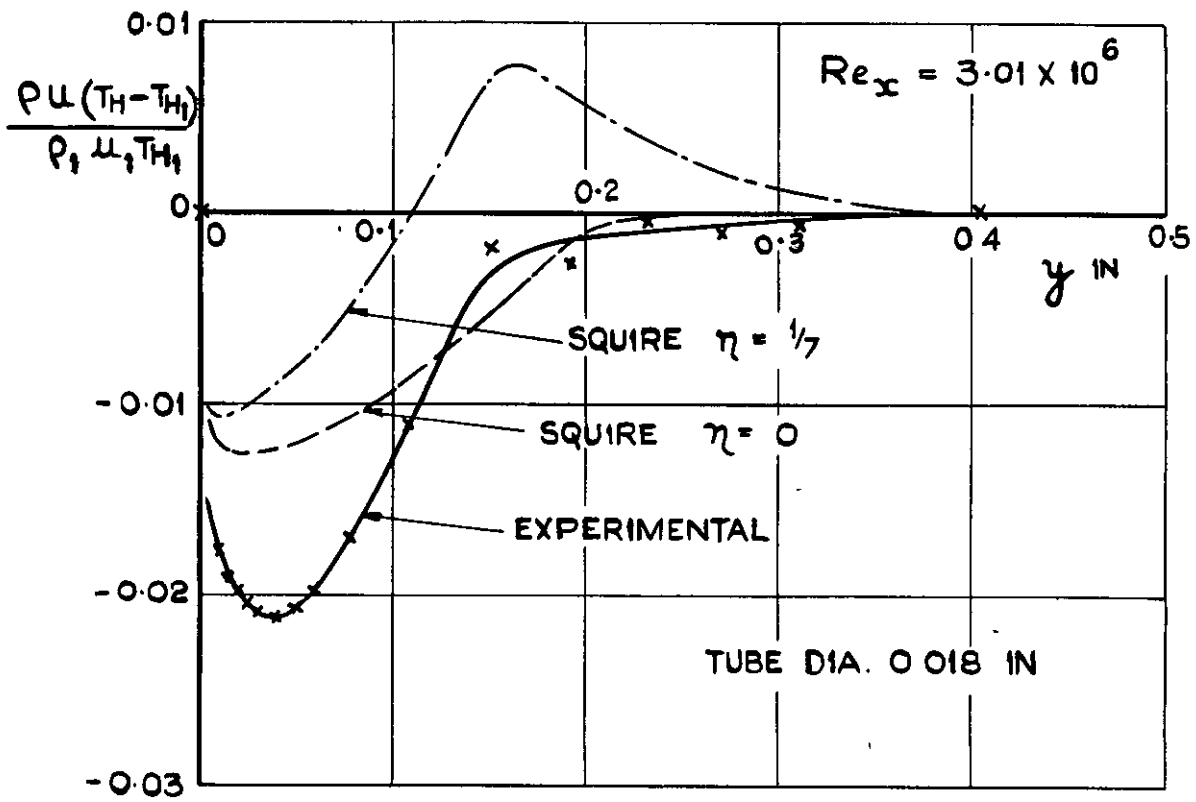

FIG. 24. ENERGY DISTRIBUTIONS ACROSS BOUNDARY LAYER UNDER ZERO HEAT TRANSFER CONDITIONS, USING VARIOUS TEMPERATURE — VELOCITY DISTRIBUTIONS (SEE FIG 23. ABOVE)

C.P. No. 139
(15,348)
A.R.C. Technical Report

PUBLISHED BY HER MAJESTY'S STATIONERY OFFICE

To be purchased from

York House, Kingsway, LONDON, W.C.2: 423 Oxford Street, LONDON, W.1
P.O. Box 569, LONDON, S.E.1
13a Castle Street, EDINBURGH, 2 | 1 St. Andrew's Crescent, CARDIFF
39 King Street, MANCHESTER, 2 | Tower Lane, BRISTOL, 1
2 Edmund Street, BIRMINGHAM, 3 | 80 Chichester Street, BELFAST
or from any Bookseller

1953

Price 12s. 0d. net

PRINTED IN GREAT BRITAIN

S.O. Code No. 23-9007-39